*In proceedings of the 90th Shock and Vibration Symposium, Shock and Vibration Exchange, www.savecenter.org, Atlanta, Georgia, November 2019.*

# Numerical simulations of large high explosive charge detonating near ground surface with shallow layer of soil before ground rock

Morgan Johansson[a,b*], Leo Laine[c], Ola Pramm Larsen[d], and Joosef Leppänen[b]

[a]Norconsult AB
Theres Svenssons gata 11, 417 55 GÖTEBORG, Sweden
*Corresponding author: morgan.johansson@norconsult.com

[b]Chalmers University of Technology
Sven Hultins gata 6, SE-412 96 GÖTEBORG, Sweden

[c]LL Engineering
Stugvägen 4, SE-438 94 HÄRRYDA, Sweden

[d]CAEwiz Consulting AS
Grinda 2B, NO-0861 OSLO, Norway

Numerical simulations have been conducted in Autodyn 2D and 3D to study how a large high explosive (HE) detonation near ground generates airblast loads. The airblast was systematically studied by comparing results with assumption of rigid ground, or with influence of different type of soils and their depths to rock. Other parametric studies carried out were the influence due to type of explosive, charge geometry and the presence of a nearby HESCO wall. The aim was to investigate, using numerical simulations in Autodyn, how accurately the propagation of the air shock wave can be predicted. These simulations were conducted independent of the results from the experimental test of a large HE detonation near ground surface within the SHIELD program.

## INTRODUCTION

The super heavy improvised explosive loading demonstration (SHIELD) test program have several countries involved: Germany, Norway, Sweden, Switzerland and the United States of America. The purpose was to conduct a very large Vehicle-borne improvised explosive device (VBIED) detonation and study the effects on physical protection solutions for both civilian and military purposes, and fortified constructions and by improving and expanding forensic data collection and assessment methodologies, see [1]. In this case, the heavy vehicle combination consisted of a tractor semitrailer laden with 37.6 tonne commercially available ammonium nitrate/fuel oil (ANFO), corresponding to approximately 30 tonne TNT equivalent. The explosion was conducted in Älvdalen, Sweden, in August 2019.

## EXPERIMENTAL SET UP AT ÄLVDALEN TEST SITE

The test area is located about 40 km north of the small town Älvdalen in Sweden, with a total prepared test area of 700 x 1 000 $m^2$ [1]. Fig. 1 shows an overview of the test-site and in Table 1 brief information of the various structures present is presented. The explosive charge consisted of a Vehicle-borne improvised explosive device (VBIED) of 37.6 tonnes ANFO placed at ground zero (GZ), see Fig. 2. At 10 m from GZ, a 4 x 4 x 80 m barrier wall of HESCO baskets, with a pyramid-like cross-section, was erected, see Fig. 3. The main structure at the test-site consisted of a reinforced concrete frame structure of four floors in which separate structural elements could be attached, see Fig. 4. This target building, denoted SKUSTA, was placed at 125 m from GZ.

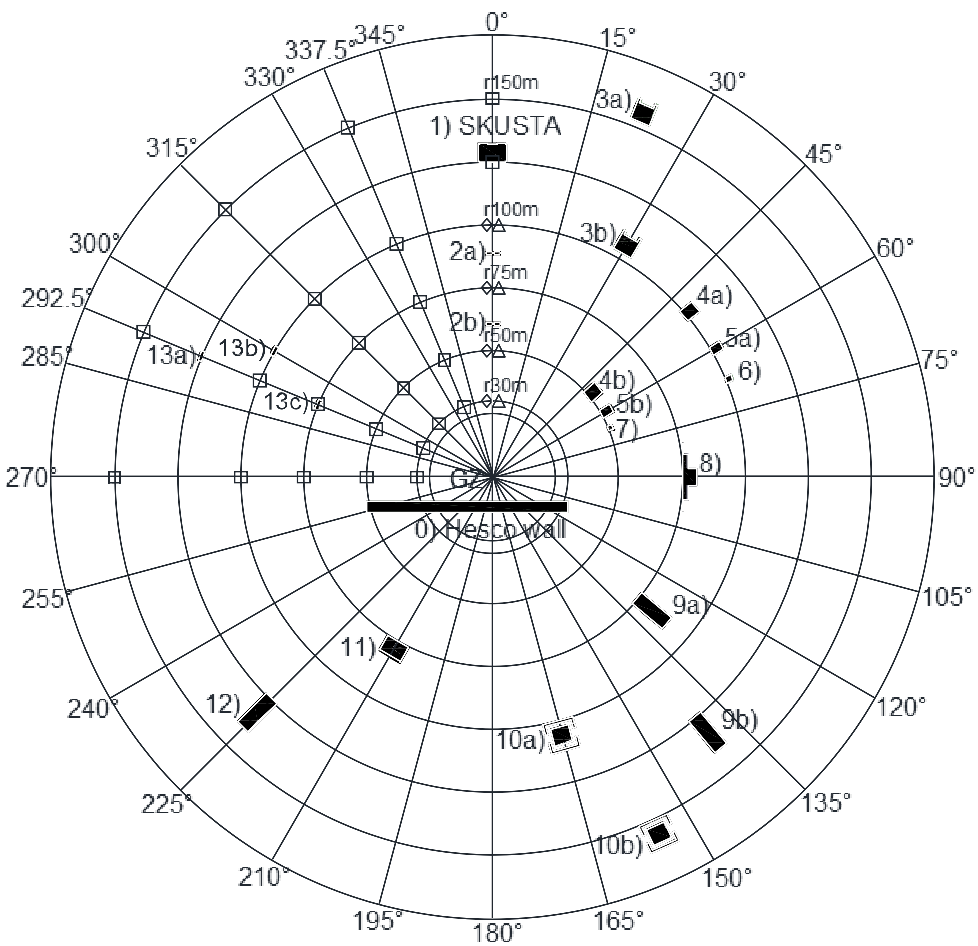


*Fig. 1 Overview of test objects. Ground Zero (GZ) perspective looking at the target building SKUSTA.*

*Table 1 Overview of test objects showing the object ID, type and approximate distance from ground zero (GZ).*

| ID | Object Name and Type | Approximate distance from GZ [m] |
|---|---|---|
| □ ◇ △ | Measuring points of Ground Surface Overpressure/ Side-on Overpressure and Total Pressure | 30/50/75/100/125/150 |
| 0) | HESCO wall (Germany) | 10 |
| 1) | SKUSTA building (Norway) | 125 |
| 2a-b) | CTGC bunkers (Switzerland) | 58/85 |
| 3a-b) | SCont container (Sweden) | 105/155 |
| 4a-b) | DCEGS shelter (Germany) | 50/100 |
| 5a-b) | DCE shelter (Germany) | 50/100 |
| 6) | DTow1 tower (Germany) | 100 |
| 7) | DISL box (Germany) | 100 |
| 8) | DTow3 large tower (Germany) | 75 |
| 9a-b) | DZCont container single (Germany) | 75/125 |
| 10a-b) | Dtent army tent (Germany) | 100/150 |
| 11) | CPMS enclosure (Switzerland) | 75 |
| 12) | D2Zcont container double (Germany) | 125 |
| 13a-c) | Cars | 75/100/125 |

*Fig. 2 The charge consisted of a semi-trailer loaded with 37.6 tonnes of ANFO. Photo used with courtesy of Forsvarsbygg, Norway.*

*Fig. 3 The HESCO wall with a pyramid-like cross section of width 4 m (bottom layer), height 4 m and length 80 m. In the photo the top level of the HESCO wall is missing; the picture is taken in an early construction stage. Correct cross-section is 4-3-2-1 HESCO baskets.*

(a) (b)

*Fig. 4 Overview of the SKUSTA building, concrete frame structure (a) without test objects (b) with test objects. Photos used with kind courtesy of Forsvarsbygg, Norway.*

## GROUND MATERIAL SAMPLES FROM THE TEST SITE

Numerical simulations involving the ground are in general very challenging due to the difficulties involved when modelling the physical behaviour of soils and rocks. The material models required to capture the nonlinear behaviour of these materials are complex and experimental data for material characterization is not easily obtained. Also, the local variations on soil composition, water content, and bedrock properties can be significant. For example, the water content of the soil can alter the physical behaviour of the ground dramatically one day to the next based on weather conditions. In order to enhance the modelling accuracy of the SHIELD experiment concerning the ground, the Norwegian Geotechnical Institute (NGI) was employed to characterize the soil at the test site. NGI has extensive experience in soil characterization and state of the art laboratory equipment that can among other things, carry out advanced tri-axial compaction tests.

In Fig. 5 an overview picture is shown of the sample locations made during July 2nd, 2019, relative to Ground Zero. The samples were extracted using NGI's 72 mm diameter steel cylinders and a sledgehammer. To get a representative set of samples based on location, various distances, polar angles, and ground depths was chosen; see white dashed line in Fig. 5. The ground, characterized as compacted moraine, was very hard and an excavator was employed to reach sample depths of 1.0 m and 0.5 m.


*Fig. 5 Ground sample location overview from a Ground Zero (GZ) perspective looking at the SKUSTA test building.*

In addition to the undisturbed cylinder samples (i.e. S01-S04), loose samples in sealed plastic bags for complementary NGI testing, was also extracted at the respective locations (i.e. S01B-S04B). In order to measure the water content present in the ground on the SHIELD test day, additional cylinder samples were obtained the day before testing, i.e. August 14th of August 2019. These samples were taken with the sole purpose of getting a representative measure of the water content in the ground, furthermore, enabling a post-experiment reconstruction of the actual water content for the planned advanced tri-axial soil tests, which is aimed to be conducted in year 2020. The tri-axial testing have been conducted earlier on different soil material, Sjöbo Sand from Sweden, see [2]-[5]. Table 2 gives a detailed overview of the specifications for the sample taking on the SHIELD test site.

*Table 2 Ground sample overview showing the sample location, depth, and other related sample specifications.*

| Ground Sample ID | Sample Type | Taken | Radius [m] | Angle [°] | Depth [cm] | Planned Tri-axial tests | Basic Testing | Early Testing [1)] | Water Content | Target Dates, NGI |
|---|---|---|---|---|---|---|---|---|---|---|
| S01 | Cylinder | 2. Jul | 5 | 315 | 5 | (•) | | | | Q1 2020 |
| S02 | Cylinder | 2. Jul | 10 | 315 | 100 | | | • | | 5. July |
| S03 | Cylinder | 2. Jul | 20 | 360 | 50 | • | | | | Q1 2020 |
| S04 | Cylinder | 2. Jul | 40 | 337.5 | 5 | (•) | | | | Q1 2020 |
| S01B | Bag | 2. Jul | 5 | 315 | 5 | | • | | | 30. Oct |
| S02B | Bag | 2. Jul | 10 | 315 | 100 | | • | | | 30. Oct |
| S03B | Bag | 2. Jul | 20 | 360 | 50 | | • | | | 30. Oct |
| S04B | Bag | 2. Jul | 40 | 337.5 | 5 | | • | | | 30. Oct |
| S03S | Bag | 2. Jul | 20 | 360 | 0 | | • | | | 30. Oct |
| S05 | Cylinder | 14. Aug | 7 | 315 | 10 | | | | • | 30. Sep |
| S06 | Cylinder | 14. Aug | 20 | 315 | 10 | | | | • | 30. Sep |
| S06 | Bag | 14. Aug | 20 | 315 | 10 | | | | • | 30. Sep |
| S06 | Cylinder | 14. Aug | 20 | 315 | 10 | | | | • | 30. Sep |

[1)] Preliminary material properties: $\rho$, G, and $v_p$ estimates.

NGI provided a basic test and estimation of soil material properties about the Älvdalen proving ground backfill [6]. The water content was about 8% during the day of testing (15th of August) and the grains size testing gave the results that the grains in Älvdalen soil is a very well graded material. The in situ density was determined to 2330 kg/m3. Further data about different soil material properties are summarized in Table 3.

*Table 3 Measured and estimated in situ and theoretical maximum density (TMD) properties of Älvdalen proving ground soil.*

| In situ properties | | | |
|---|---|---|---|
| Porosity | $\varphi = 20$ % | Depth of burial | $Z = 3$ m |
| Water content | $w = 8$ % | Poisson´s ratio | $\nu = 0.25$ |
| Depth of burial | $D = 3$ m | Initial shear modulus | $G_{\max} = 162$ MPa |
| Void ratio | $e = 0.25$ | Shear wave velocity | $C_s = 264$ m/s |
| Degree of saturation | $Sr = 86$ % | Initial constr. modulus | $M_{\max} = 487$ MPa |
| Dry density | $\rho_{dry} = 2160$ kg/m$^3$ | Compressive wave velocity | $C_p = 457$ m/s |
| In situ density – moist | $\rho_{total} = 2330$ kg/m$^3$ | | |
| **Theoretical maximum density (TMD) properties** | | | |
| Porosity | $\varphi_{TMD} = 17.8$ % | Bulk modulus | $K_{TMD} = 8.53$ GPa |
| Void ratio | $e_{TMD} = 0.22$ | Sound velocity | $C_{TMD} = 1886$ m/s |
| Saturation - implicit | $S_{r,TMD} = 100$ % | | |
| Mass density | $\rho_{TMD} = 2398$ kg/m$^3$ | | |

## 2D and 3D FE-MODELS

The modelling and simulations where conducted with the AUTODYN simulation software, see [7], both in 2-dimensional (2D) and 3-dimensional (3D) versions. The computational hardware was a PC with 16 CPUs with dual socket Xeon 3.2 GHz base frequency processors (E5-2687WV2) and with ram 128 GB.

### *AIR AND EXPLOSIVE MATERIAL MODELLING*

The air was modelled with an ideal gas law with initial density of 1.225 kg/m$^3$. The air was pressurized to one atmosphere, i.e. 101.33 kPa. The internal energy was set to 206.8 kJ/kg. Initial studies were conducted with both TNT equivalent weight with density 1 630 kg/m$^3$and ANFO weight of 37.6 tonnes with density 842 kg/m$^3$ and using the Jones-Wilkins-Lee equations. In accordance with [8] an equivalence factor of 0.82 was used to determine the TNT charge weight, resulting in an equivalent charge weight of 30.8 tonnes of TNT and a total charge of approximately 130 GJ. The influence of different charge shapes was studied: hemispherical charge, spherical charge, cylindrical charge and a charge consisting of multiple vertical cylindrical charges, see Fig. 6.

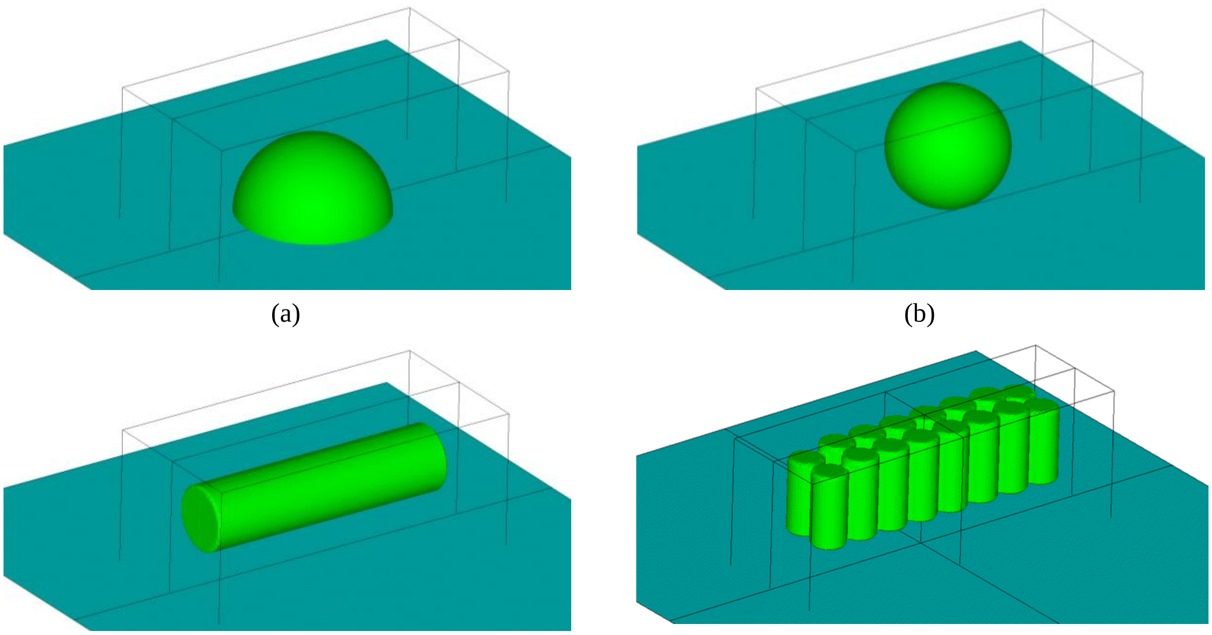

(a) (b) (c) (d)

*Fig. 6 Geometrical shapes used in the analyses: (a) hemispheric charge; (b) spherical charge; (c) horizontal cylindrical charge; and (d) multiple vertical cylindrical charges.*

The hemispherical charge was made in two variants, one with TNT with radius 2.2 m and one with ANFO with radius 2.7 m; both located on the ground surface. The spherical charge was based on ANFO with radius 2.1 m with the centre of gravity located 2.5 m above ground. The ANFO was modelled according to the data sheet of the type used, see [9]. More details about ANFO JWL parameters are given in [10] and in Table 4 the parametric values used for the explosives in the numerical simulations are summarised.

*Table 4 JWL parameters for explosives used in the numerical simulations.*

| Explosive | $A$ | $B$ | $R_1$ | $R_2$ | $w$ | $D_{C\text{-}J}$ | $P_{C\text{-}J}$ |
|---|---|---|---|---|---|---|---|
| | [GPa] | [GPa] | [-] | [-] | [-] | [m/s] | [GPa] |
| TNT [1)] | 37.4 | 3.75 | 4.15 | 0.90 | 0.35 | 6 930 | 21 |
| ANFO-1 [1)] | 49.5 | 1.89 | 3.9 | 1.12 | 0.33 | 4 160 | 5.2 |
| ANFO-2 [2)] | 267 | 3.44 | 7,04 | 1.16 | 0.39 | 3 850 | 3.3 |

1) Default values in Autodyn.

2) Values based on explosive Prillit A in [10]. This explosive was chosen since its density of 850 kg/m$^3$ best corresponded to that of ANFO Exan.

The cylindrical shape was based on ANFO in which the cylinder's length was 9.6 m and its radius was 1.2 m; its centre of gravity was placed 2.5 m above ground. This shape was a chosen approximation of the charge shape in the physical experiments in Älvdalen, where the charge was piled in a manner similar to that shown in Fig. 6d, compare with Fig. 2. In the hemispherical and spherical charges, one single detonation point was used. For the horizontal cylinder and multiple vertical cylinders, though, a total of four detonation points were used, located in the middle, 2.5 m above ground, at positions of $x = 0$ m at -3.6 m, -1.2 m, 1.2 m, and 3.6 m, see Fig. 7.

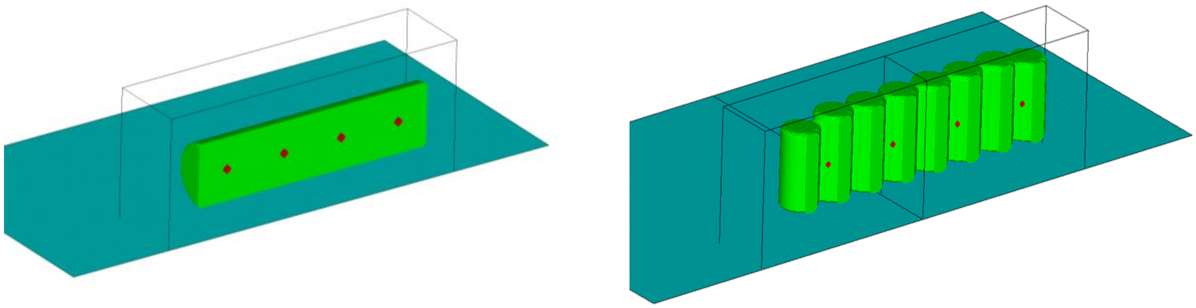

(a) (b)

*Fig. 7 Location of detonations points in (a) cylindrical charge, and (b) multiple vertical cylindrical charges.*

To approximately take into account the effect of a large mass located in the front of the semi-trailer (i.e. its engine), a rigid object with a mass of 2 000 kg was included in the 3D analyses of the horizontal cylinder as shown in Fig. 8. It was found that the effect of this rigid mass was not negligible, see SIMULATIONS RESULTS, and hence it was also included in the final FE analyses (including the parametric study of the influence of the HESCO wall).

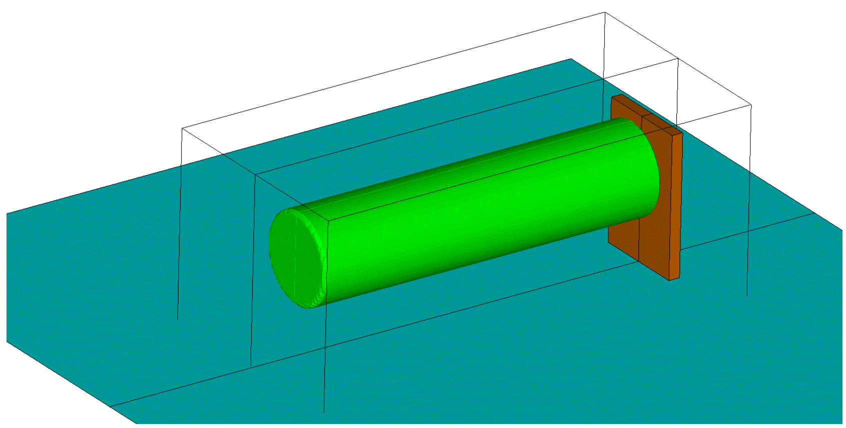

*Fig. 8 Inclusion of a rigid mass 2 000 kg, approximately simulating the effect of the semi-trailer's engine, in the 3D model with a cylindrical charge. The rigid mass was located in direction α = 90°.*

## *SOIL AND ROCK MODELLING*

In FE analyses of explosions, the ground surface is often approximated as a rigid surface, i.e. perfect reflexion occurs to the ground surface and no energy is lost into the ground. In this study, though, the effect of including the ground surface was further investigated and the soil material was modelled using a Porous Compaction EoS with Mo granular strength. Apart from Älvdalen soil, a sand material (Sjöbo sand) was also used as comparison. In Table 5 the input data for the soil materials are listed. For the rhiolit bedrock a von Mises material model was used with the following parameters: $\rho = 2\,500$ kg/m$^3$, $G = 10$ GPa, $\nu = 0.18$, $\sigma_Y = 10$ MPa.

*Table 5 Input data for Älvdalen soil and Sjöbo sand used in the numerical simulations (left: compaction curve; right: linear unloading curves).*

Älvdalen soil

| $\rho$ [kg/m³] | $P$ [MPa] |
|---|---|
| 2 330 | 0 |
| 2 340 | 1.15 |
| 2 360 | 12 |
| 2 400 | 65 |
| 2 440 | 160 |
| 2 482 | 300 |

| $\rho$ [kg/m³] | $c$ [m/s] |
|---|---|
| 2 330 | 340 |
| 2 335 | 480 |
| 2 344 | 866 |
| 2 350 | 1 140 |
| 2 365 | 1 461 |
| 2 398 | 1 886 |
| 2 600 | 1 886 |

Sjöbo sand

| $\rho$ [kg/m³] | $P$ [kPa] |
|---|---|
| 1 674 | 0 |
| 1 740 | 4.58 |
| 1 874 | 15 |
| 1 997 | 29 |
| 2 144 | 59 |
| 2 250 | 98 |
| 2 380 | 179 |
| 2 485 | 289 |
| 2 585 | 450 |
| 2 671 | 651 |

| $\rho$ [kg/m³] | $c$ [m/s] |
|---|---|
| 1 674 | 265 |
| 1 746 | 852 |
| 2 086 | 1 722 |
| 2 147 | 1 876 |
| 2 300 | 2 265 |
| 2 572 | 2 956 |
| 2 598 | 3 112 |
| 2 635 | 4 600 |
| 2 641 | 4 634 |
| 2 800 | 4 634 |

## *2D FE MODELS*

2D FE analyses were carried out for conceptual studies of the influence of the following parameters:

- **Type of explosive:** Using a hemispherical charge, according to Fig. 6a, a charge of TNT were compared with two types of ANFO: ANFO-1 and ANFO-2. The former is the default ANFO type used in Autodyn, while ANFO-2 correspond to ANFO Exan, which was what was used in the test.
- **Type and depth of soil material:** Using a spherical charge according to Fig. 6b the rigid ground surface was replaced with a soil material (Älvdalen moraine and Sjöbo sand) of various depths (2.5 m, 5.0 m or infinite depth). Below the soil layer material, a von Mises plastic model was used to model the Rhiolit bedrock, see Fig. 9 Illustration of 2D model used to study the influence of the ground material. The soil material was modelled as Älvdalen moraine or Sjöbo sand.Fig. 9. In these analyses the charge consisted of ANFO-2.

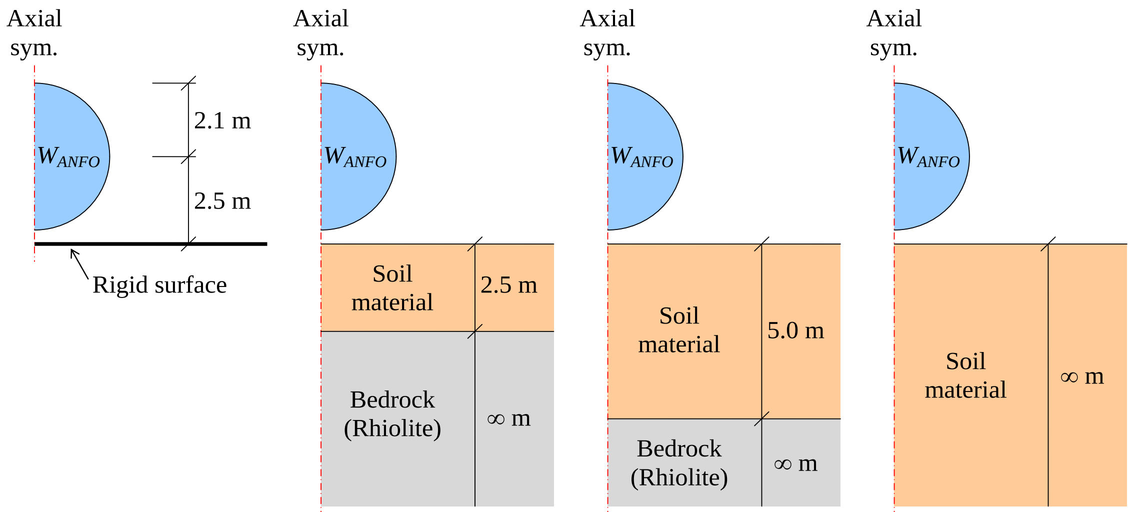


*Fig. 9 Illustration of 2D model used to study the influence of the ground material. The soil material was modelled as Älvdalen moraine or Sjöbo sand.*

## *3D FE MODELS*

3D FE analyses were carried out both for conceptual studies and for the final analyses that are to be compared with experimental results. In the conceptual studies the influence of the following parameters were studied:

- Cylindrical charge versus multiple vertical cylindrical charges, see Fig. 6c and d. These analyses were made with ANFO-1.
- Inclusion of rigid mass, simulating the semi-trailer's engine, see Fig. 8, using a charge made of ANFO-2.
- HESCO wall, modelled as rigid, deformable or non-existing, see Fig. 3, using a charge made of ANFO-2.
- Movement of cars at various distances from GZ due to resulting blast load.

All the objects shown in Fig. 1, i.e. SKUSTA, bunkers, containers, cars etc., were modelled in Autodyn 3D, see Fig. 10. Furthermore, result points at the locations of pressure gauges used in the test were included in the model for future comparison with the experiments. In Fig. 10 and Fig. 11 the locations of the result points, representing the main pressure gauges on ground and SKUSTA, respectively, is shown. A full presentation of all result points defined in the model is made in Appendix I.

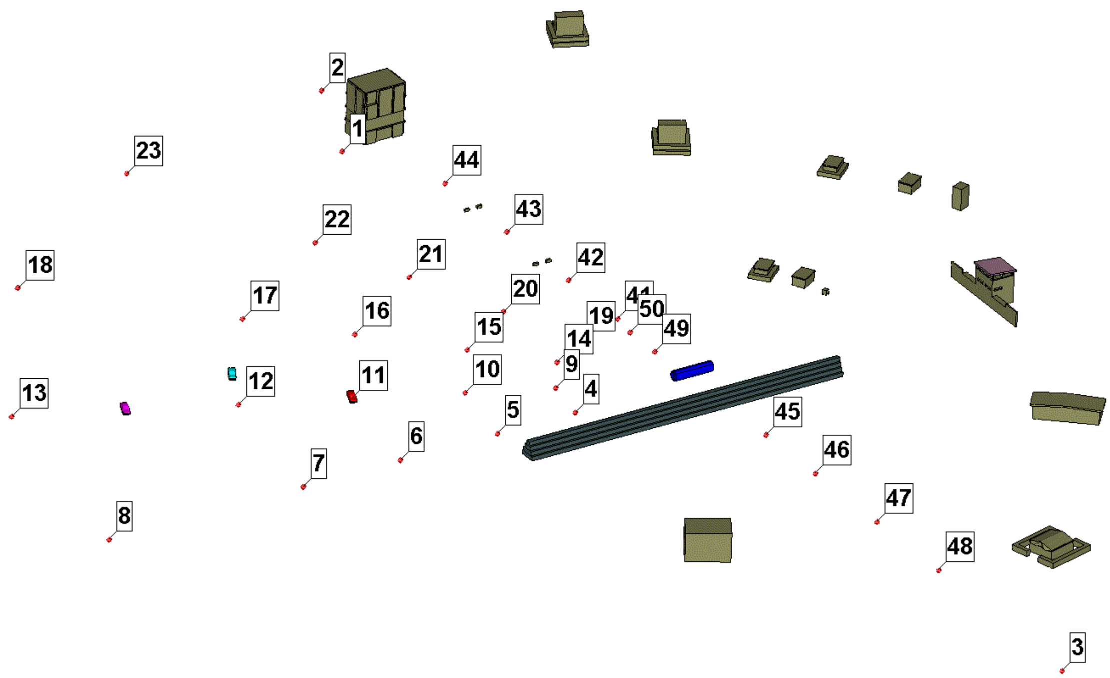


*Fig. 10 3D FE-model of the test objects with location of result points in FE model marked, representing the main pressure gauges on ground used in test.*

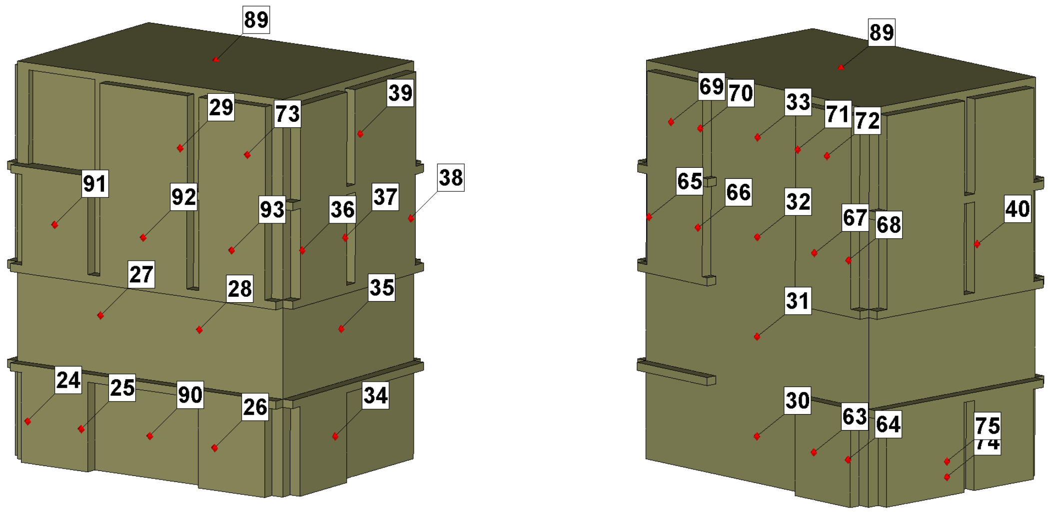


(a) (b)

*Fig. 11 Building SKUSTA including detail shape of the structure surface (a) is front view; (b) back view. Numbered red marks indicate position of result points in the FE model, representing pressure gauges used in test.*

The HESCO wall was modelled both as a rigid surface and as a deformable entity that could be broken up by the acting blast load using an erosion model. To study its effect on the final blast load the wall was in one analysis fully removed.

In the final analysis of the SHIED test set-up a total of three cars were included in the model. The cars were modelled as rigid by using solid elements, see Fig. 12. The same shape was used for all the cars, regardless of real type, but the correct mass, and centre of gravity position were modelled as close to the real vehicle model type as possible. This was done by using different fill densities in the volume elements, i.e. higher density in the lower part of the car (car platform and engine) and lower density in the upper part (passenger compartment). At a distance 75 m from GZ, an Opel Corsa was modelled that had a total weight of 900 kg and at 100 m an Audi A6 was positioned with an estimated weight of 1500 kg. A third car, Citroen C6 with mass 1500 kg, was modelled at distance 125 m. The movement of the cars were measured in two points: front and back.

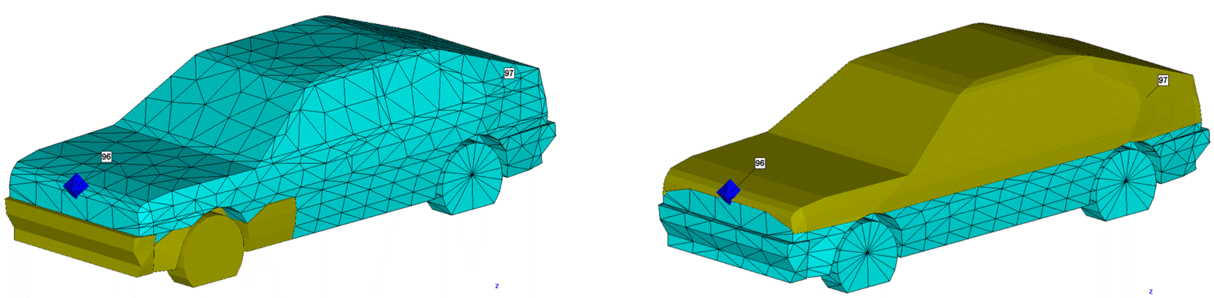


(a) (b)

*Fig. 12 Overview of the car model used in the FE analyses: (a) high density region; (b) low density region.*

### *FE MODELING TECHNIQUE*

The main simulation techniques to handle both near and far field accuracy are to use re-mapping techniques. Initially, multi-material Euler was used during detonation until shock wave propagation was properly initiated; after this remapping into Euler Flux Corrected Transport (FCT) elements were used to accurately simulate the airblast. To achieve good accuracy, both in near field ground shock propagation, cratering, and ground vibrations, an Arbitrary Eulerian Lagrangian (ALE) formulation was used for the soil and ground rock with Fluid Structure Interaction (FSI).

2D axisymmetric multi-material Euler was initially used until 0.5 ms before the shock wave hit the ground. Remapping to 3D FCT Euler was then used. The largest 3D models, as shown in Fig. 10, included different fine mesh resolution zones with a cell size of 0.25 m cubic elements. This to avoid too much smoothing of the peak pressures. However, the total impulse intensity was still deemed to be accurate described also when using the coarser mesh. Geometric coarsening with ratio 1.1 was used outside measurement zone with defined result points to avoid reflections from the mesh. Again, all measurements done in fine zone this meant that different models focused on different sectors and radius distances. The largest possible model consisted of 60 million cells which was a hardware limit of the PC, see beginning of this section for hardware details. Approximately 25 simulations were needed to reach all points of interest in experimental sectors 360 degrees with a 150 m radius. For the result points located at 250 m radius, a medium resolution zone with cell size 0.50 mm was used. To improve computational efficiency 3D remapping was also used. The main result points (within 150 m from GZ) are shown in Fig. 10; a full description of all result points defined in the FE analyses are presented in Appendix I.

## SIMULATION RESULTS

### *PARAMETRIC STUDIES*

In Fig. 13 the influence of different charge explosives is compared. Here, the overpressure and impulse intensity of 2D analyses, with a hemispherical charge geometry according to Fig. 6a, are compared at a distance of 50 m and 100 m. From this it can be observed that the 30.8 tonnes of TNT and 37.6 tonnes of ANFO-1 generate similar results; hence indicating that the equivalent factor of 0.82 used is a good approximation. As a comparison it can be mentioned that the load obtained in ConWep [8] for this load situation (i.e. 2·30.8 = 61.6 tonnes TNT for a spherical free-air burst) gives $P^+$ = 549 kPa (116 kPa) and $i^+$ = 5 600 Pas (2 950 Pas) at a distance of 50 m (100 m). Hence, the maximum pressures obtained in the FE analyses are close to that predicted in ConWep while the impulse intensities are about 30% (20%) lower than predicted in ConWep. The latter difference is in line with previous observations in e.g. [11] and is hence expected. It can also be noted that there is a difference between ANFO-1 and ANFO-2. However, this is due to the difference in energy content of the two explosives and consequently, the characteristics of the ANFO used is of importance.

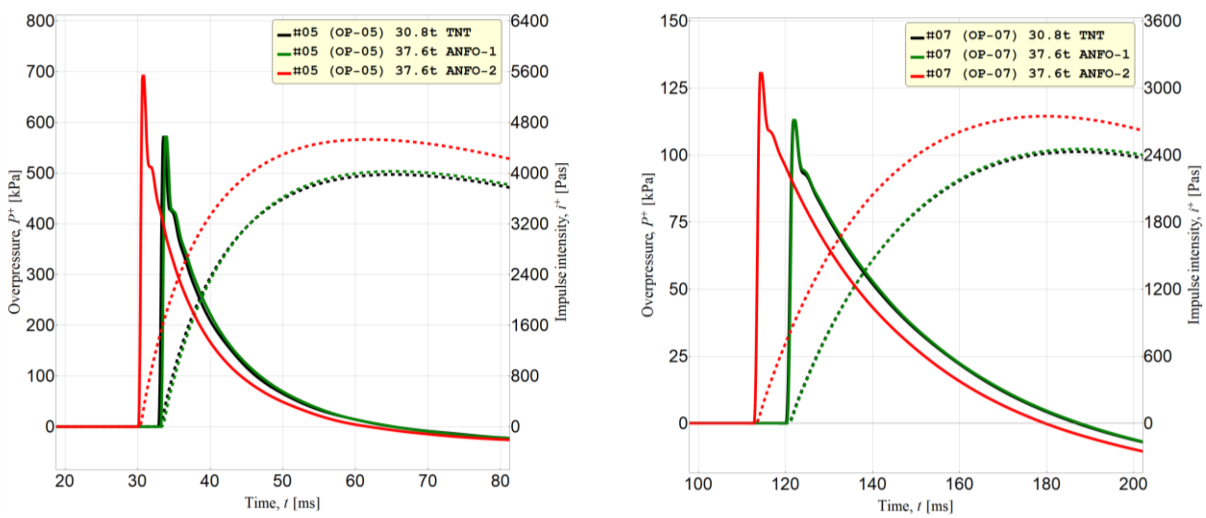


$r$ = 50 m    $r$ = 100 m

*Fig. 13 Influence of charge explosive; comparison of overpressure and impulse intensity for 2D analyses of various type of explosives when using a spherical charge.*

In Fig. 14 the resulting overpressure and impulse intensity is compared at a distance of 50 m and 100 m från GZ when the ground has been modelled as shown in Fig. 9, using Älvdalen soil. It was found that the influence of the ground material was small and that its depth had negligible effect. The same observations were also made when using Sjöbo sand as ground material. In Fig. 15 a similar comparison is made, but now with Älvdalen soil and Sjöbo sand, and a minor difference can then be seen. In Fig. 16 the ground deformations 350 ms after detonation is shown; i.e. the final deformations obtained will still be a function of both the type and depth of the ground material. It was found that the total energy from the high explosive that was transmitted to the ground was around 2 % and 3 % for Älvdalen and Sjöbo, respectively, see Table 6.

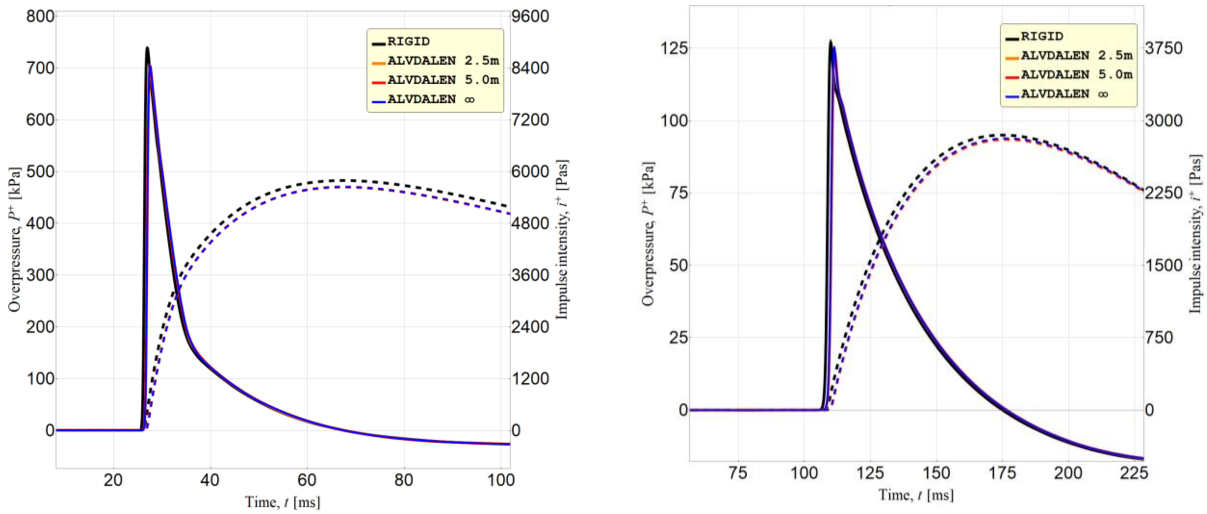


$r$ = 50 m $\qquad$ $r$ = 100 m

*Fig. 14 Influence of ground material depth; comparison of overpressure and impulse intensity for 2D analyses of a spherical charge when using Älvdalen soil.*

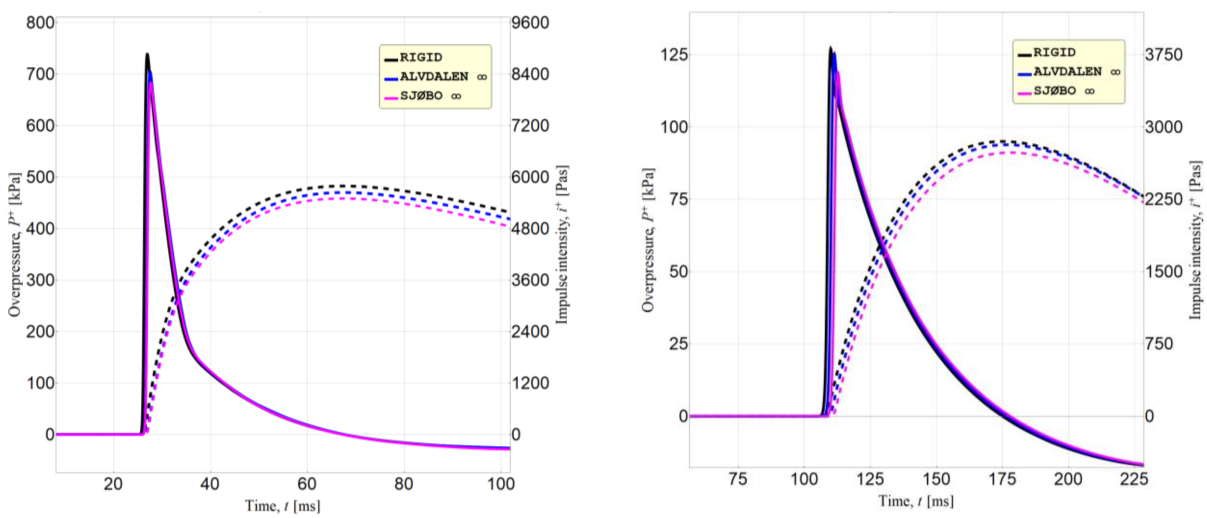


$r$ = 50 m $\qquad$ $r$ = 100 m

*Fig. 15 Influence of ground material; comparison of overpressure and impulse intensity for 2D analyses of various ground material (depth ∞ m).*

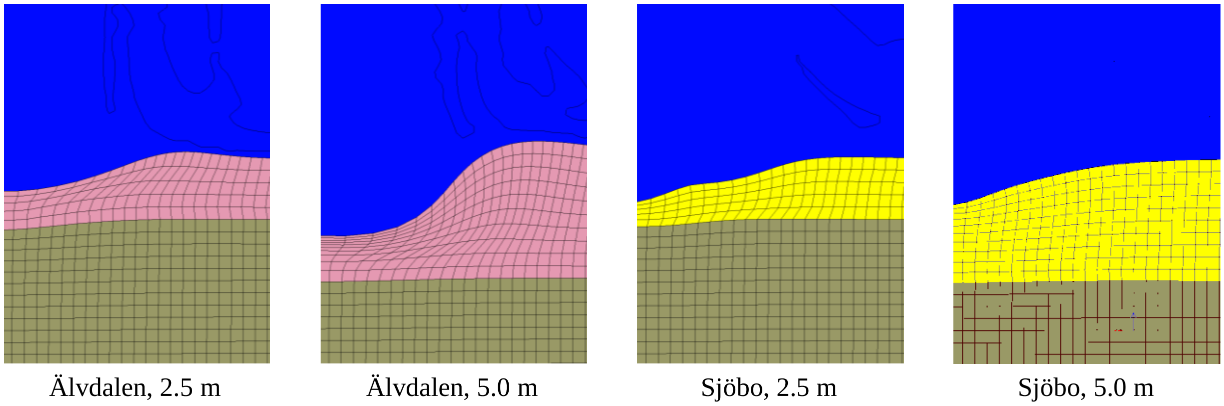


*Fig. 16 Ground deformations 350 ms after detonation for various type and depth of ground material. At this time step the movement of the ground has all but stopped and the deformations shown are close to the final ones. The left edges of the plots correspond to the axial symmetry line in the 2D model; compare with Fig. 9.*

*Table 6 Total Ground energy (kinetic + internal energy), as percentage of total high explosive energy.*

| | Soil depth = 2.5 m | | | Soil depth = 5.0 m | | | Soil depth = ∞ m | | |
|---|---|---|---|---|---|---|---|---|---|
| Soil material | Surface [%] | Bedrock [%] | Total [%] | Surface [%] | Bedrock [%] | Total [%] | Surface [%] | Bedrock [%] | Total [%] |
| Älvdalen | 1.8 | 0.6 | 2.3 | 2.1 | 0.3 | 2.4 | 2.3 | 0 | 2.3 |
| Sjöbo | 2.7 | 0.3 | 2.9 | 2.9 | 0.1 | 2.9 | 2.9 | 0 | 2.9 |

In Fig. 17 the influence of charge geometry are compared. Here, the overpressure and impulse intensity of 2D and 3D analyses, with charge geometry according to Fig. 6a to Fig. 6c are compared at a distance of 50 m and 100 m when the charge consists of ANFO-2. For the cylindrical charge, results are presented both perpendicular ($\alpha = 0°$) and parallel ($\alpha = 270°$) to its axis without (sym) and with (asym) the presence of a rigid mass, see Fig. 8. From this it can be observed that a cylindrical charge, at a distance of 50 m, produce significantly larger load in the main direction ($\alpha = 0°$) compared to that obtained from a hemispherical or spherical charge. In the perpendicular direction ($\alpha = 270°$), though, the load is almost identical for the hemispherical and cylindrical charges. However, this good correspondence seems to be a coincidence; since at an increased distance of 100 m, a clear difference between hemispherical charge and cylindrical charge in the perpendicular direction has appeared. The influence of the rigid mass is negligible at a distance of 50 m and at distance of 100 m its effect is still small. Nevertheless, the effect of the rigid mass is still included in the further analyses.

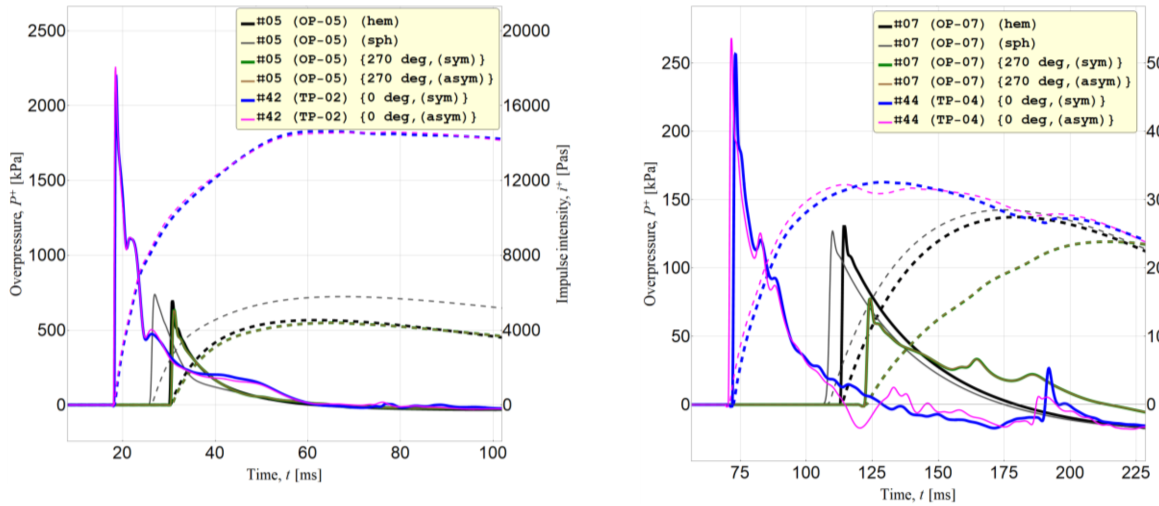


*r* = 50 m　　　　　　　　　*r* = 100 m

*Fig. 17 Influence of charge geometry; comparison of overpressure and impulse intensity for 2D and 3D analyses of a hemispherical, spherical and cylindrical charge. Results for the cylindrical charge without (sym) and with (asym) a rigid mass are presented.*

In Fig. 18 a comparison is made of the influence of whether the charge is modelled as a horizontal cylinder or of multiple vertical cylindrical charges as shown in Fig. 6c and Fig. 6d, respectively. These analyses were made with ANFO-1 and it can be noticed that there are some differences in the maximum overpressure but that the impulse intensities are very similar. However, for such high overpressures the impulse intensity is critical and hence, it is deemed to be an acceptable simplification to model the charge in the SHIELD test set-up as a horizontal cylinder.

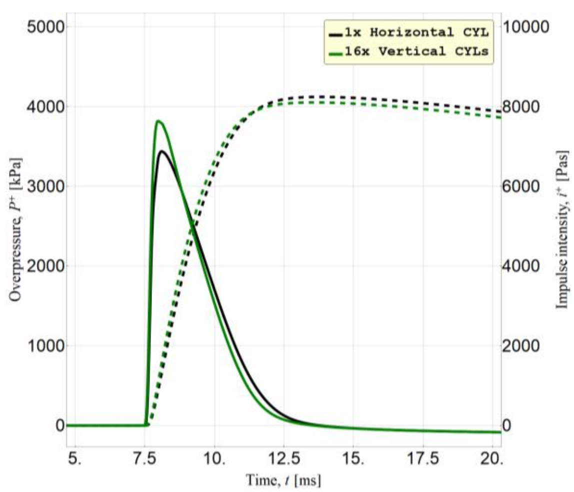


*r = 25 m, α =* 0°

*Fig. 18 Influence of charge geometry; comparison overpressure and impulse intensity when charge is shaped as a horizontal cylinder versus multiple vertical cylindrical charges. ANFO-1 was used as explosive.*

In Fig. 19 the influence of the HESCO wall is compared in result points located in front of the wall; both of how the wall is modelled (rigid or deformable HESCO) or whether it is not present at all (no HESCO). From this it can be concluded that, at a distance of 50 m or 100 m, the presence of the wall has negligible effect on the pressure and impulse intensity in a point perpendicular to the wall (i.e. $\alpha$ =0°). However, for a point located in the direction parallel to the wall (i.e. $\alpha$ =270°), there is a considerable influence on the load, resulting in increased overpressure and impulse intensity at 50 m from GZ. This is an effect of the partial confinement provided by the wall. For a point far away from the wall, though, this effect has vanished; this is e.g. partly the case at 100 m when $\alpha$ =270°. From Fig. 19 it can also be noticed that it has very little effect whether the wall is modelled as rigid or as deformable.

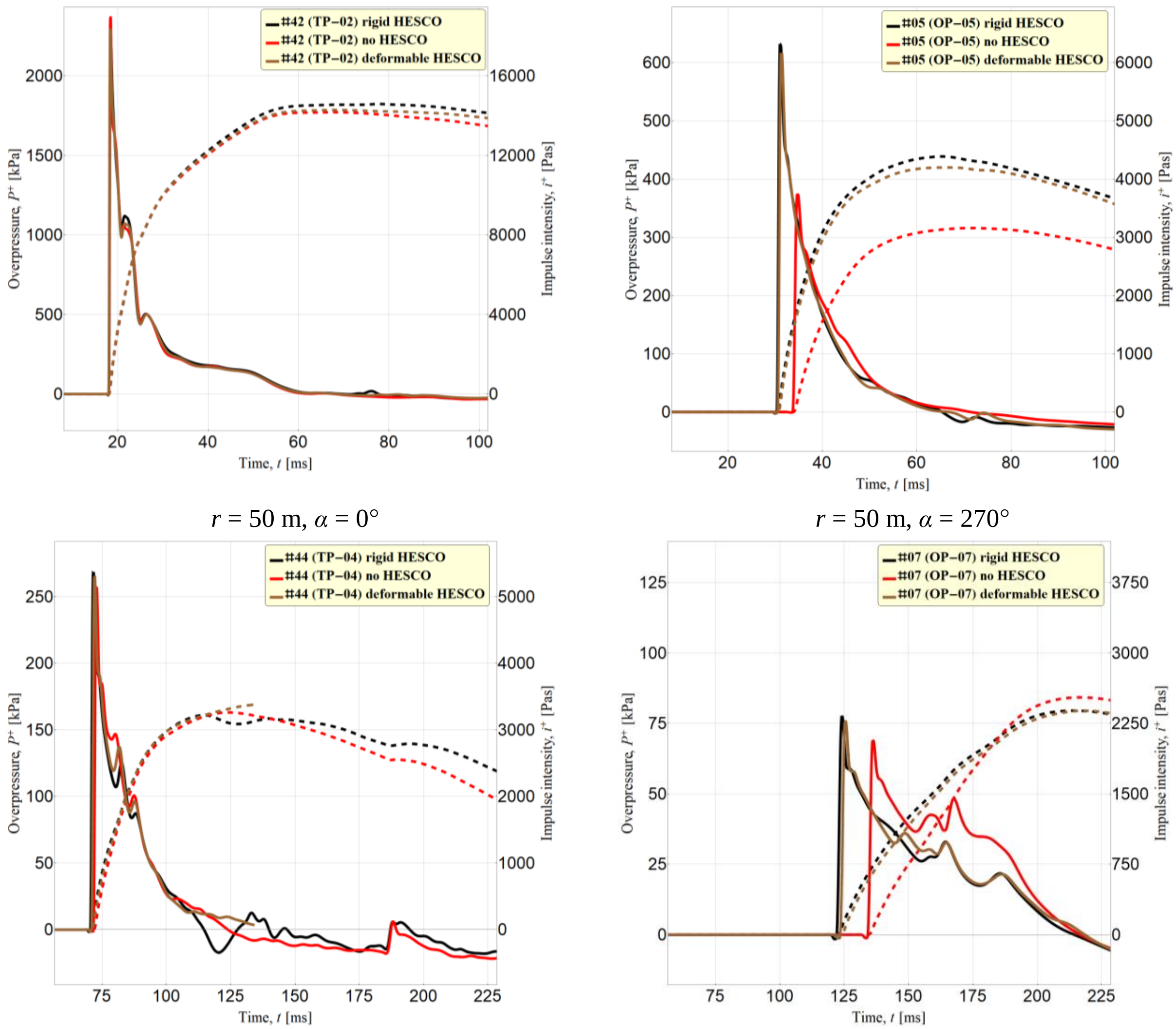


*Fig. 19 Influence of HESCO wall; comparison of overpressure and impulse intensity in front of wall at $\alpha$ = 0° and 270° when it is modelled as rigid, deformable or as no wall at all.*

In Fig. 20 the influence of the HESCO wall is compared in result points located behind the wall when the wall is modelled as rigid or not present at all. As expected, it is evident that the wall has a major influence of the resulting load; the effect being larger at a smaller distance from GZ.

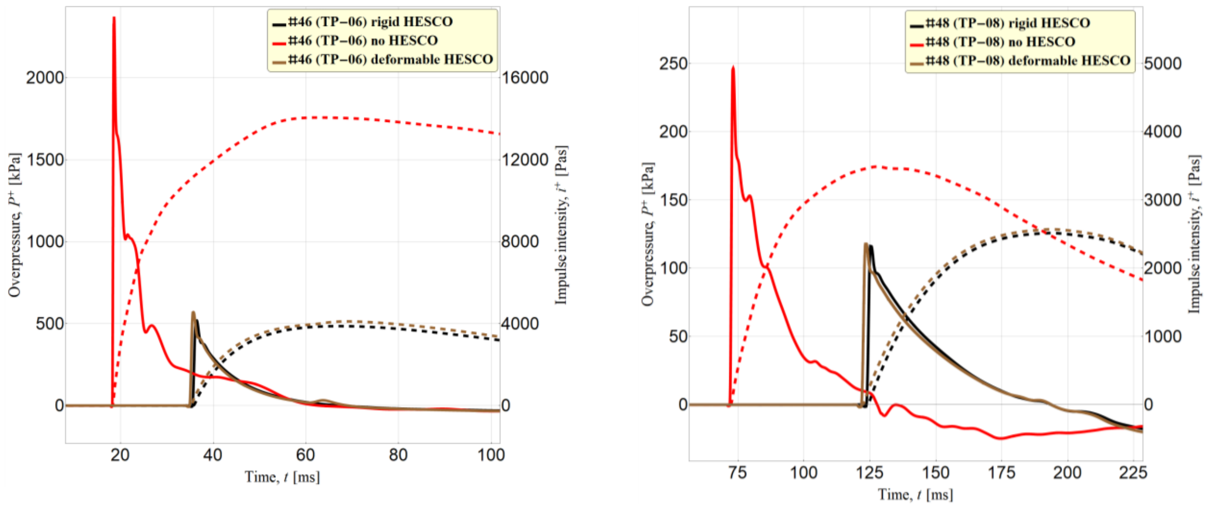


$r$ = 100 m, $\alpha$ = 0° $r$ = 100 m, $\alpha$ = 270°

*Fig. 20 Influence of HESCO wall; comparison of overpressure and impulse intensity behind wall at α = 180° when it is modelled as rigid, deformable or as no wall at all.*

*ANALYSIS OF SHIELD TEST SET-UP*

Based on the conceptual analyses the settings for the final analysis of the test set-up is possible. This analysis was carried out with the following assumptions:

- Horizontal cylindrical charge of 37.6 tonnes ANFO-1I with a rigid mass simulating the semi-trailer's engine, see Fig. 8.
- Ground surface and HESCO wall modelled with rigid surfaces (deformable material were used for an analysis finished after about 150 ms).

In Fig. 21 the resulting blast wave propagation is shown for the first 120 ms after detonation. In these plots, the HESCO wall was modelled using a deformable HESCO wall and it can be noted that the wall has obtained a notable deformation after about 20 to 40 ms; after 120 ms the wall deformation is locally several meters.

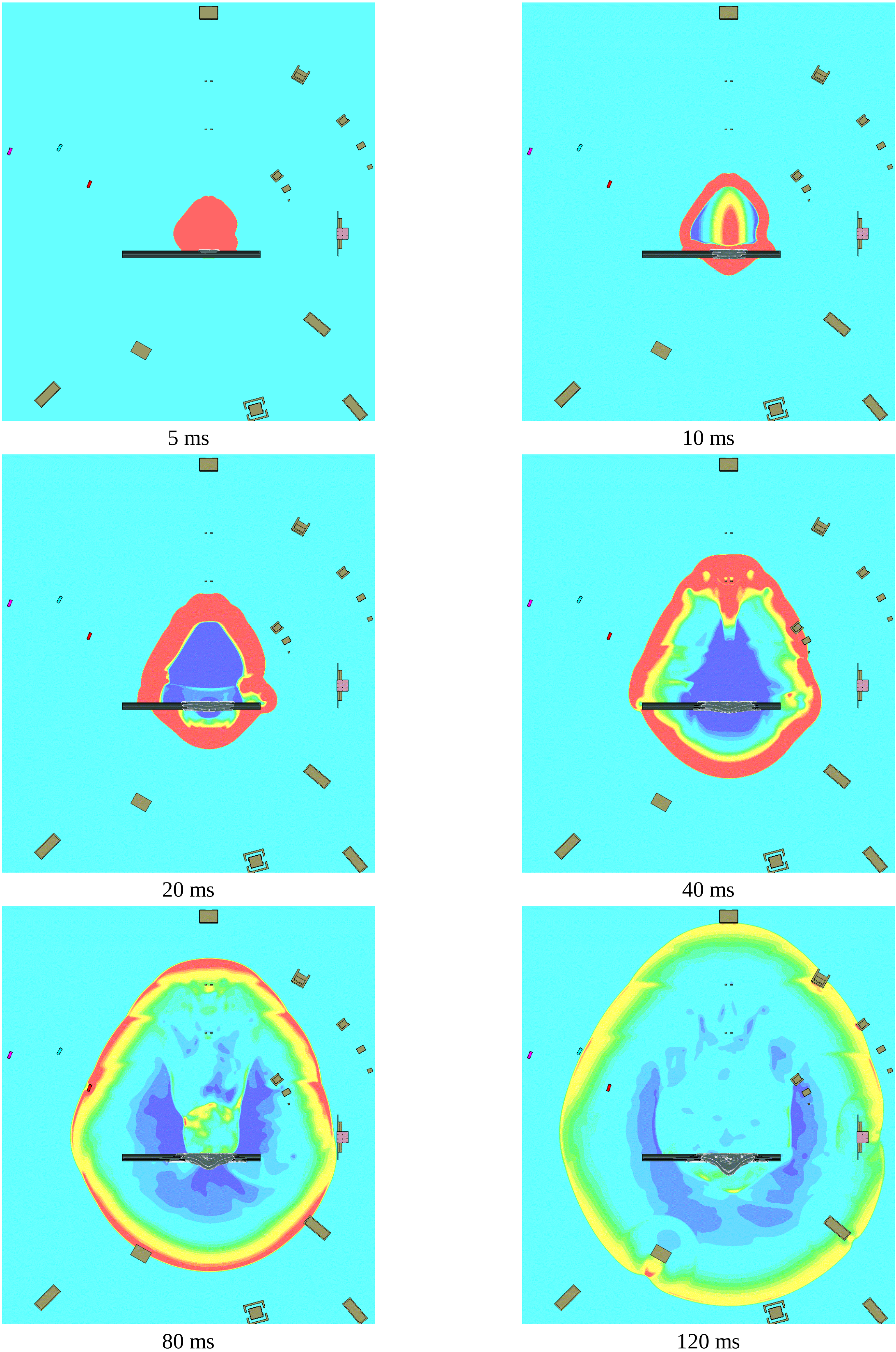


*Fig. 21 Blast wave propagation (pressure) in analysis of SHIELD test; the HESCO wall was here modelled as deformable.*

In Fig. 22 and Fig. 23 the overpressure and impulse intensity are compared for various result points located on ground and at SKUSTA, respectively. From this it can be noted that the load are significantly higher, at a distance of 50 m and 75 m from GZ, in the main direction ($\alpha$ = 0°) than in a perpendicular ($\alpha$ = 270°) or diagonal angle ($\alpha$ = 315°). At 100 m the pressure is still higher in the main direction, but the impulse intensity no longer differs that much. At 150 m the results are similar independent of direction; here, though, the result point in the main direction is shielded by SKUSTA. For loads in all the result points in the FE model, see Appendix II.

In Fig. 24 the movement of the two cars closest to GZ are presented. In the FE analysis, Car 1 (closest to GZ, and least weight) tipped over because of the blast load. Car 3 produced a response like that of Car 2 but with a maximum movement of about 40 mm.

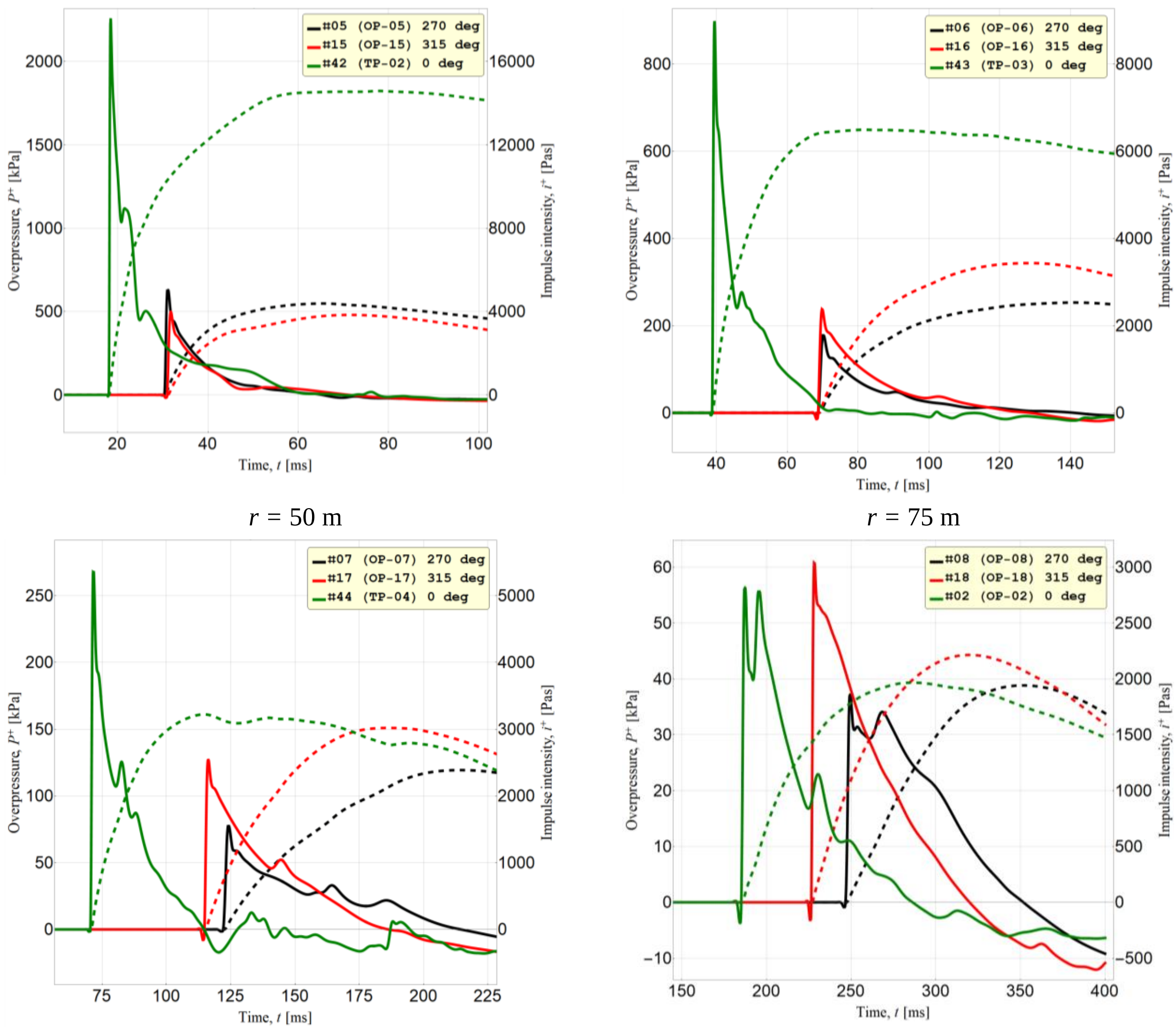


*Fig. 22 SHIELD test set-up; comparison of overpressure and impulse intensity for α = 0°, 270° and 315° at a distance of 50-150 m. Note that point #02 (r= 150 m) is shielded by SKUSTA. See Fig. 10 for detailed location of result points.*

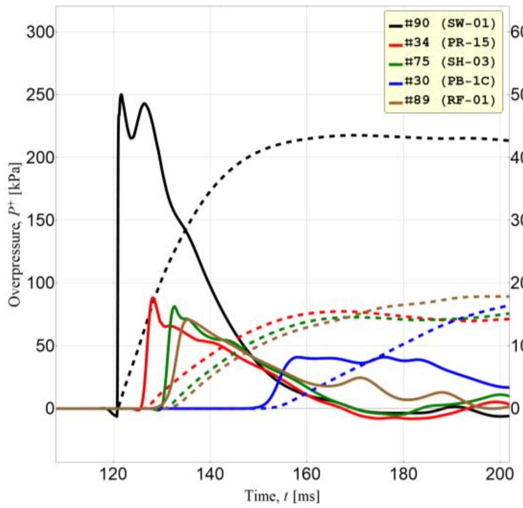


Floor 1

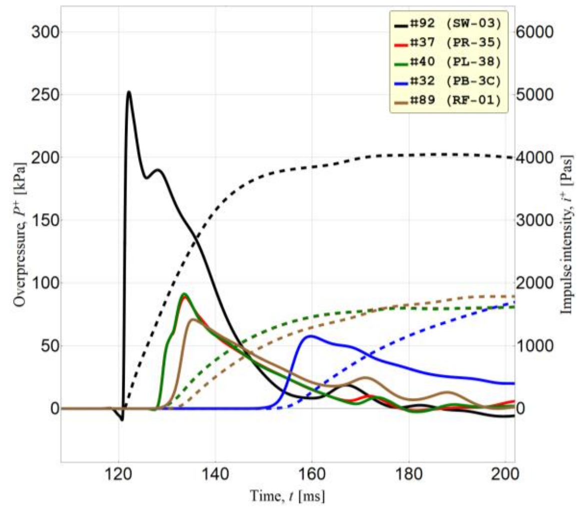


Floor 3

*Fig. 23 SHIELD test set-up; comparison of overpressure and impulse intensity for front (#90, #92), side (#34, #75, #34, #40), back (#30, #32) and roof (#89) of SKUSTA. See Fig. 11 for detailed location of result points.*

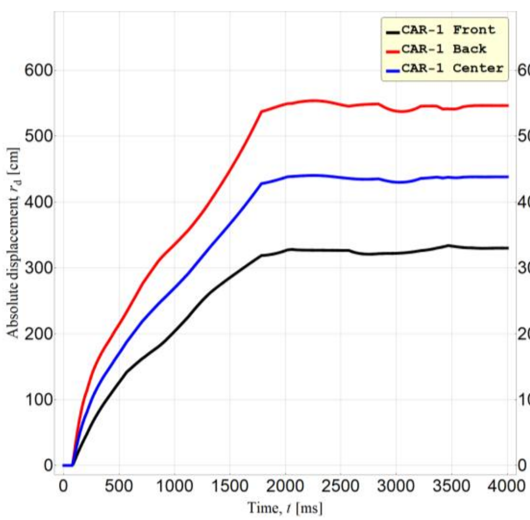


Car 1

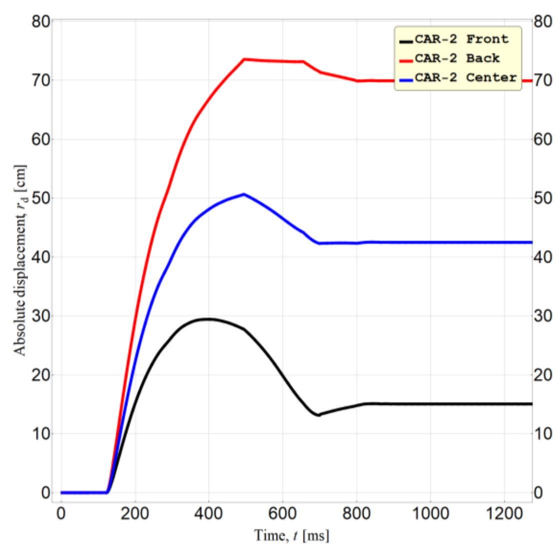


Car 2

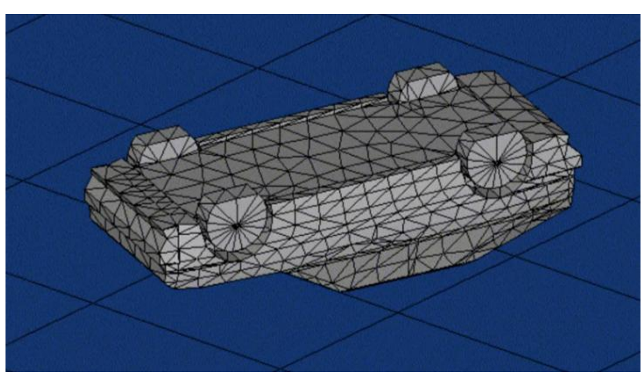

Car 1 upside-down after test

*Fig. 24 Movement of Car 1 and 2 due to the explosion in the SHIELD test set-up. In the FE analysis, Car 1 tipped over and ended upside-down due to the force caused by the blast wave.*

## CONCLUSIONS AND FUTURE WORK

In this paper, numerical simulations of a large high explosive charge (30 tonne TNT equivalent, carried by a tractor semitrailer), detonating near ground surface, have been carried out in Autodyn. Several parametric studies were made i.e. type of charge explosive, type and depth of soil material, charge geometry, and HESCO wall located close to the charge:

- **Type of explosive:** It was found that using an equivalent weight factor of 0.82 for TNT and ANFO-1 (default in Autodyn) was a good approximation. However, the use of ANFO-2 (simulating ANFO Exan) resulted in increased loads; hence, indicating that the characteristics of the ANFO used is of importance.

- **Type and depth of soil material:** The influence of the soil material was small and depending on the soil material assumed about 2-3% of the released explosion energy transferred into the ground. The soil depth, though, had negligible influence. Hence, when the charge is located close above ground, it is a good assumption to treat the ground as a rigid surface.

- **Charge geometry:** Charge geometry can have a substantial effect on the resulting load. However, it was found suitable to approximate the current charge as a horizontal cylinder.

- **HESCO wall:** The presence of a wall had negligible influence on the load in front of the wall in the perpendicular direction. However, in the parallel direction, the presence of the wall had a large effect. For the load behind the wall, the presence of the wall also had a large effect. In all cases it had negligible effect whether the wall was modelled as rigid or deformable, hence indicating that using a rigid wall is a good assumption.

Based on these parametric studies, a simulation of the SHIELD test set-up was made and pressure time relations determined. These results are presented in the paper and will in future work be compared with the results obtained in the test.

## ACKNOWLEDGEMENTS

The authors acknowledge the support given by MSB and especially Lars Gråbergs, who is member of the West Coast Sweden Shock Wave Group (WCSSWG).

## REFERENCES


[1] Rickman D., Jaun M., Knutsen T., Dirlewanger H., and Persson A. (2017): ” An Introduction to the Super Heavy Improvised Explosive Loading Demonstration (SHIELD) Test Program, *Proceedings of the 88th Shock and Vibration Symposium*, Jacksonville, Florida, USA.

[2] Laine L. and Sandvik A. (2001): “Derivation of mechanical properties for sand”, *4th Asian-Pacific conference on Shock and Impact Loads on Structures, CI-Premier PTE LTD*, vol. 4, pp 353-360, Singapore.

[3] Heyerdahl H. and Madshus C. (2000): “EOS-data for sand, Tri-axial tests on sand from Sjöbo”, Norges Geotekniske institutt (NGI), NGI rept. 20001157-1, Oslo, Norway.

[4] Laine L. and Larsen O.P. (2012): “Implementation of Equation of State for Dry Sand in Autodyn”, *83rd Shock and Vibration Symposium, Shock and Vibration Exchange (SAVE)*, New Orleans, LA.

[5] Laine L. (2012): *Markstötvåg* (Ground Shock. In Swedish). Swedish Civil Contingencies Agency, Publ. no MSB344, Karlstad, Sweden.

[6] Madshus C. (2019): *Testfield in Älvdalen – Measured and estimated properties of the ground soil* (in Norwegian), Norges Geotekniske institutt (NGI), NGI rept. 20001157-1, Oslo, Norway.

[7] Century Dynamics Inc. (2004*): AUTODYN Theory Manual Revision 5.0*, San Ramon, CA, USA.

[8] ConWep (1992): Collection of conventional weapons effects calculations based on TM 5-855-1, Fundamentals of Protective Design for Conventional Weapons, U.S. Army Engineer Waterways Experiment Station, Vicksburg, USA.

[9] ORICA (2018): “TECHNICAL DATA SHEET Exan™ E and Exan™ EA Packaged ANFO – Sweden”, *Orica Sweden AB*, publication date 2018-03-27, Nora, Sweden.

[10] Sanchidrián J., Castedo R., López L, Segarra P., Santos A. (2015): “Determination of the JWL Constants for ANFO and Emulsion Explosives from Cylinder Test Data”, *Central European Journal of Energetic Materials*, 2015, 12(2), 177-194, ISSN 1733-7178.

[11] Johansson J. and Laine L. (2012): *Bebyggelsens motståndsförmåga mot extrem dynamisk belastning, Del 1: Last av luftstötvåg* (*The resistance of housing settlement subjected to extreme dynamic loading. Part 1: Load of shock wave in air*. In Swedish.), Swedish Civil Contingencies Agency, Publ. no. MSB449, Karlstad, Sweden.

## APPENDIX I – PRESSURE GAIGES IN FE MODEL OF SHIELD TEST SET-UP

In this appendix, the location of the result points defined in the FE model of the SHIELD test set-up are presented.

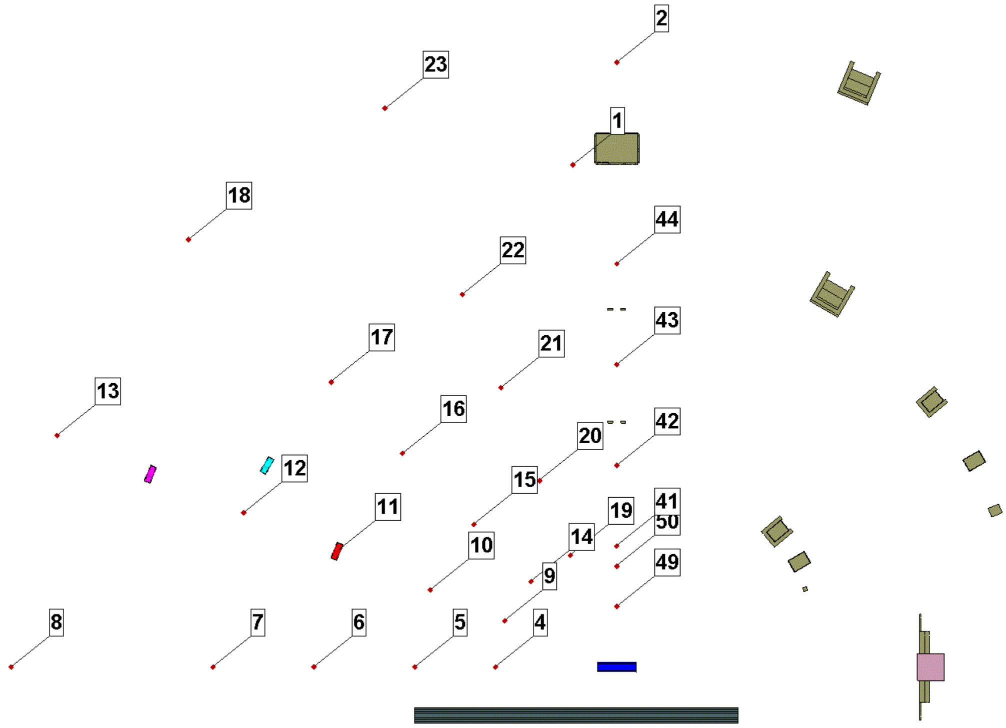


*Fig. 25 Result points on ground in front of the HESCO wall.*

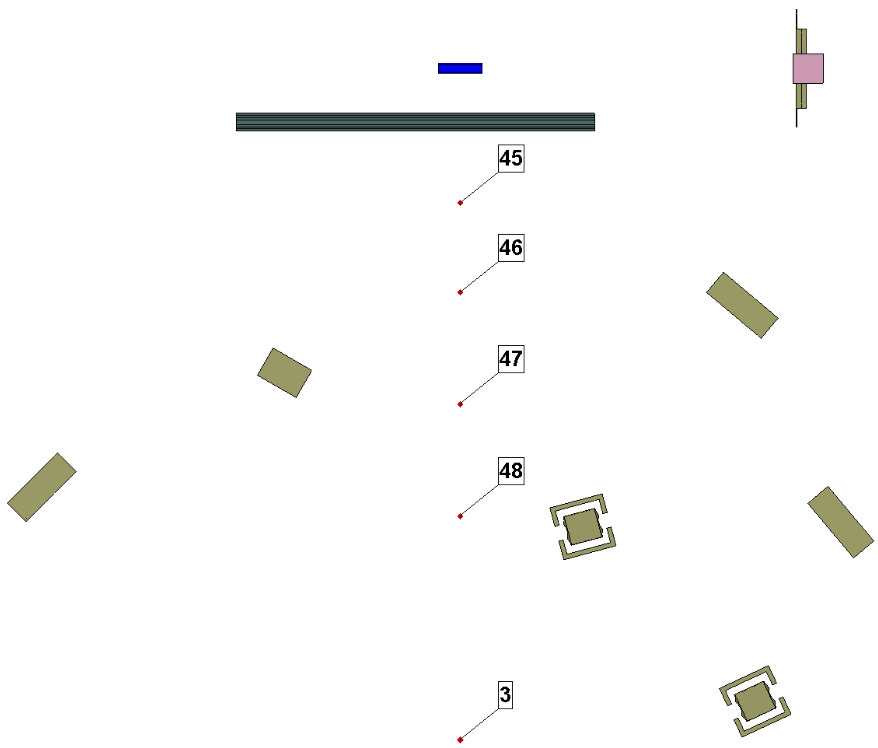


*Fig. 26 Result points on ground behind the HESCO wall.*

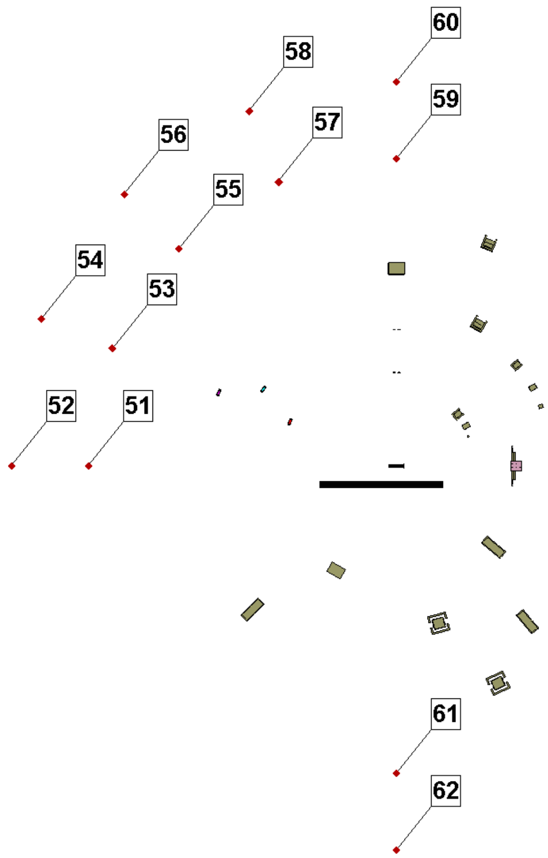


*Fig. 27 Result points on ground in the far-range field.*

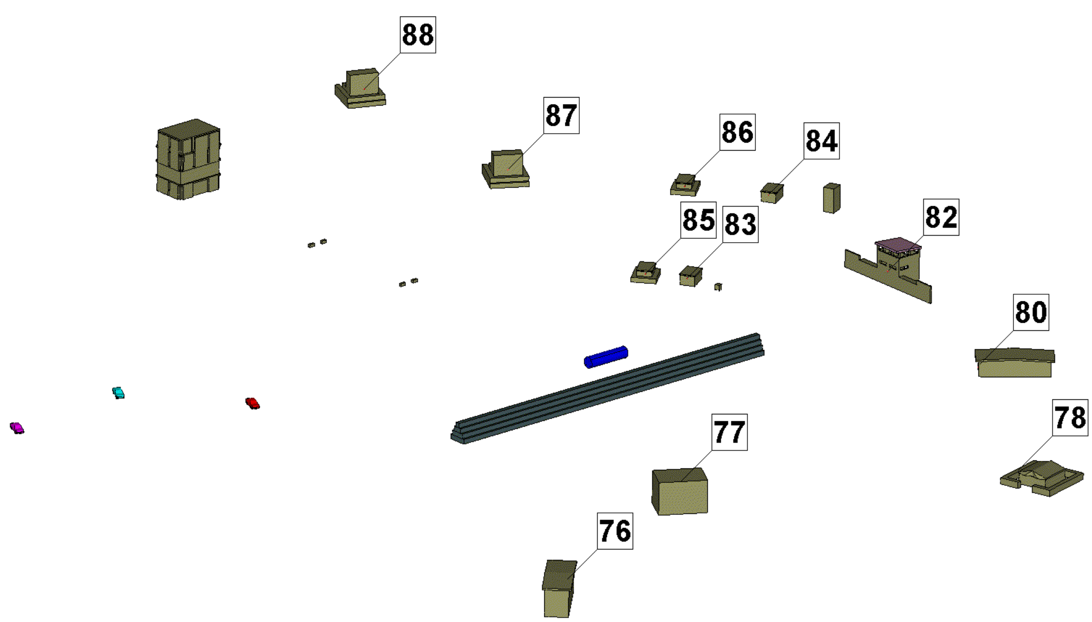


*Fig. 28 Result points located on nearby objects.*

*Table 7 Total Ground energy (kinetic + internal energy), as percentage of total high explosive energy.*

| Tracker no. | Sensor ID | Range, $r$ [m] | Angle, $\alpha$ [°] | Elevation, $z$ [m] |
|---|---|---|---|---|
| 1 | *OP-01* | 125 | 355 | 0.05 |
| 2 | *OP-02* | 150 | 0 | 0.05 |
| 3 | *OP-03* | 150 | 180 | 0.05 |
| 4 | *OP-04* | 30 | 270 | 0.05 |
| 5 | *OP-05* | 50 | 270 | 0.05 |
| 6 | *OP-06* | 75 | 270 | 0.05 |
| 7 | *OP-07* | 100 | 270 | 0.05 |
| 8 | *OP-08* | 150 | 270 | 0.05 |
| 9 | *OP-09* | 30 | 292.5 | 0.05 |
| 10 | *OP-10* | 50 | 292.5 | 0.05 |
| 11 | *OP-11* | 75 | 292.5 | 0.05 |
| 12 | *OP-12* | 100 | 292.5 | 0.05 |
| 13 | *OP-13* | 150 | 292.5 | 0.05 |
| 14 | *OP-14* | 30 | 315 | 0.05 |
| 15 | *OP-15* | 50 | 315 | 0.05 |
| 16 | *OP-16* | 75 | 315 | 0.05 |
| 17 | *OP-17* | 100 | 315 | 0.05 |
| 18 | *OP-18* | 150 | 315 | 0.05 |
| 19 | *OP-19* | 30 | 337.5 | 0.05 |
| 20 | *OP-20* | 50 | 337.5 | 0.05 |
| 21 | *OP-21* | 75 | 337.5 | 0.05 |
| 22 | *OP-22* | 100 | 337.5 | 0.05 |
| 23 | *OP-23* | 150 | 337.5 | 0.05 |
| 24 | *PF-11* | 124.7 | 358 | 1.35 |
| 25 | *PF-12* | 124.6 | 359 | 1.35 |
| 26 | *PF-13* | 124.6 | 1 | 1.36 |
| 27 | *PF-22* | 125 | 359 | 5 |
| 28 | *PF-23* | 125 | 1 | 5 |
| 29 | *PF-43* | 124.6 | 1 | 10.85 |
| 30 | *Pb-1C* | 132.2 | 0 | 1.5 |
| 31 | *Pb-2C* | 132.2 | 0 | 4.7 |
| 32 | *Pb-3C* | 132.2 | 0 | 7.9 |
| 33 | *Pb-4C* | 132.2 | 0 | 11.1 |
| 34 | *PR-15* | 127.5 | 2 | 1.6 |
| 35 | *PR-25* | 128.3 | 2 | 4.86 |
| 36 | *PR-34* | 125.6 | 3 | 7.9 |
| 37 | *PR-35* | 128 | 2 | 7.9 |
| 38 | *PR-36* | 131.6 | 2 | 7.9 |
| 39 | *PR-45* | 128.8 | 2 | 11.1 |
| 40 | *PL-38* | 128 | 358 | 7.9 |
| 41 | *SP-01* | 30 | 0 | 1.01 |
| 42 | *SP-02* | 50 | 0 | 1.01 |
| 43 | *SP-03* | 75 | 0 | 1.01 |
| 44 | *SP-04* | 100 | 0 | 1.01 |
| 45 | *SP-05* | 30 | 180 | 1.01 |
| 46 | *SP-06* | 50 | 180 | 1.01 |
| 47 | *SP-07* | 75 | 180 | 1.01 |
| 48 | *SP-08* | 100 | 180 | 1.01 |
| 49 | *NF-01* | 15 | 0 | 0.05 |
| 50 | *NF-02* | 25 | 0 | 0.05 |

| Tracker no. | Sensor ID | Range, $r$ [m] | Angle, $\alpha$ [°] | Elevation, $z$ [m] |
|---|---|---|---|---|
| 51 | *BG-01* | 200 | 270 | 0.05 |
| 52 | *BG-02* | 250 | 270 | 0.05 |
| 53 | *BG-03* | 200 | 292.5 | 0.05 |
| 54 | *BG-04* | 250 | 292.5 | 0.05 |
| 55 | *BG-05* | 200 | 315 | 0.05 |
| 56 | *BG-06* | 250 | 315 | 0.05 |
| 57 | *BG-07* | 200 | 337.5 | 0.05 |
| 58 | *BG-08* | 250 | 337.5 | 0.05 |
| 59 | *BG-09* | 200 | 0 | 0.05 |
| 60 | *BG-10* | 250 | 0 | 0.05 |
| 61 | *BG-11* | 200 | 180 | 0.05 |
| 62 | *BG-12* | 250 | 180 | 0.05 |
| 63 | *PW-01* | 132.6 | 359 | 1.5 |
| 64 | *PW-02* | 132.7 | 358 | 1.5 |
| 65 | *PB-36* | 132.7 | 2 | 7.9 |
| 66 | *PW-03* | 132.6 | 1 | 7.9 |
| 67 | *PW-04* | 132.6 | 359 | 7.9 |
| 68 | *PB-37* | 132.7 | 358 | 7.9 |
| 69 | *PW-05* | 132.6 | 2 | 11.1 |
| 70 | *PW-06* | 132.6 | 1 | 11.1 |
| 71 | *PW-07* | 132.6 | 359 | 11.1 |
| 72 | *PW-08* | 132.6 | 358.5 | 11.1 |
| 73 | *SH-01* | 124.7 | 1.8 | 10.95 |
| 74 | *SH-02* | 129.3 | 358 | 0.6 |
| 75 | *SH-03* | 129.3 | 358 | 1.1 |
| 76 | *D2ZCo* | 124.9 | 225 | 1.1 |
| 77 | *CPMS1* | 74.9 | 210 | 3.1 |
| 78 | *DTen1* | 99.9 | 165 | 0.6 |
| 79 | *DTen2* | 149.9 | 155 | 0.6 |
| 80 | *DZCo1* | 74.9 | 130 | 1.1 |
| 81 | *DZCo2* | 124.9 | 140 | 1.1 |
| 82 | *DTow3* | 75.0 | 90 | 3.01 |
| 83 | *DCE01* | 49.9 | 60 | 1.6 |
| 84 | *DCE02* | 99.9 | 60 | 1.6 |
| 85 | *DCEG1* | 49.9 | 50 | 1.6 |
| 86 | *DCEG2* | 99.9 | 50 | 1.6 |
| 87 | *SCon1* | 104.4 | 30 | 3.1 |
| 88 | *SCon2* | 154.4 | 22.5 | 3.1 |
| 89 | *RF-01* | 128.6 | 0 | 12.81 |
| 90 | *SW-01* | 125.0 | 0 | 1.35 |
| 91 | *SW-02* | 124.7 | 358 | 7.8 |
| 92 | *SW-03* | 124.6 | 0 | 7.8 |
| 93 | *SW-04* | 124.7 | 2 | 7.8 |
| 94 | CAR1F | 75 | 292.5 | 0.5 |
| 95 | CAR1B | 75 | 292.5 | 0.5 |
| 96 | CAR2F | 100 | 300 | 0.5 |
| 97 | CAR2B | 100 | 300 | 0.5 |
| 98 | CAR3F | 125 | 292.5 | 0.5 |
| 99 | CAR3B | 125 | 292.5 | 0.5 |

## APPENDIX II – PRESSURE AND IMPULSE INTENSITY IN RESULT POINTS

In this appendix, overpressure and impulse intensity are shown for all result points presented in Appendix I. The results were obtained using a horizontal cylindrical charge of 37.6 tonnes ANFO-1I with a rigid mass simulating the semi-trailer's engine, see Fig. 8. Further, the ground surface and HESCO wall were modelled using rigid surfaces.

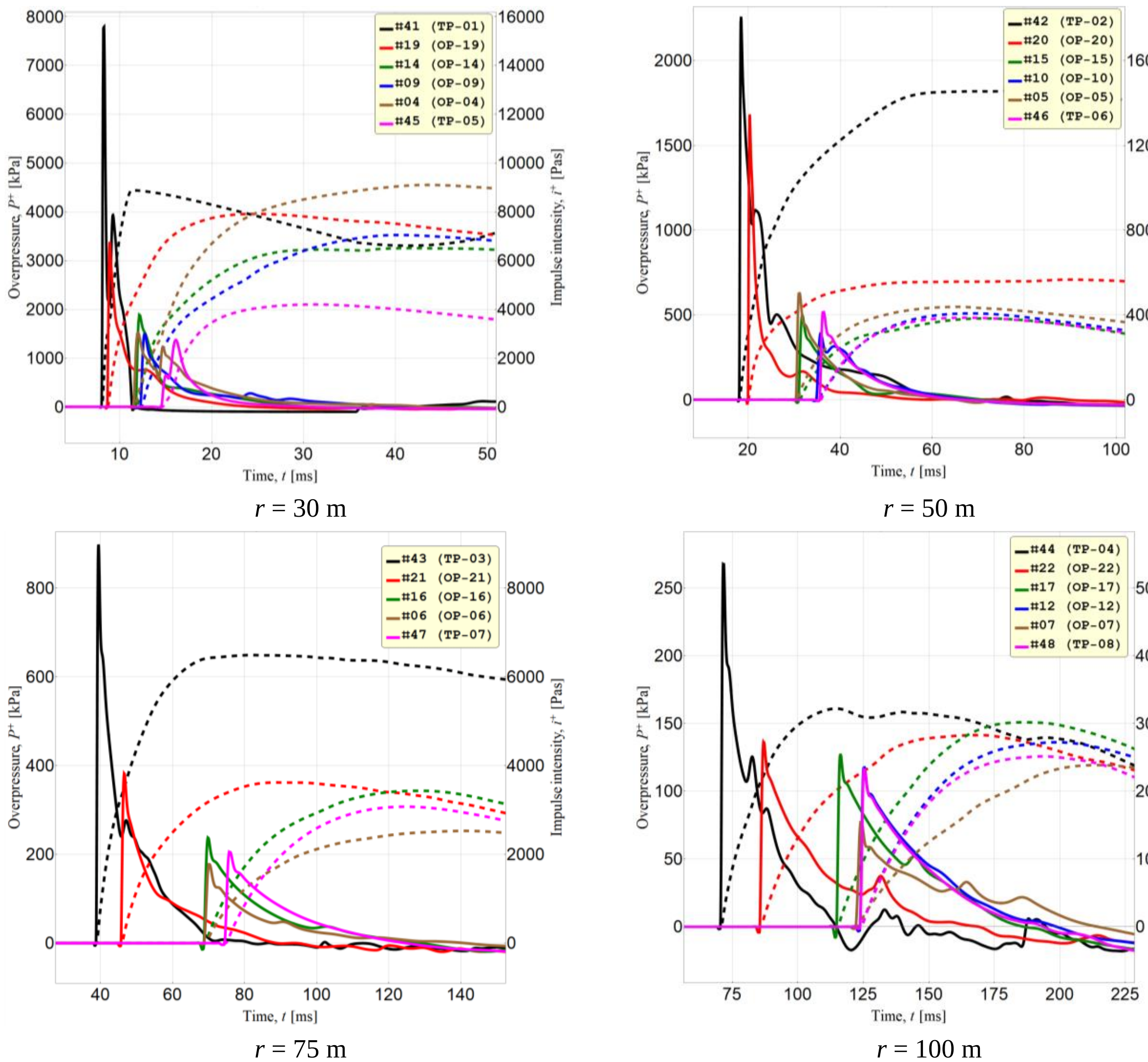


*Fig. 29 SHIELD test set-up; comparison of overpressure and impulse intensity for result points on ground at distance 30-100 m from GZ. See Fig. 25 to Fig. 28 for detailed location of result points.*

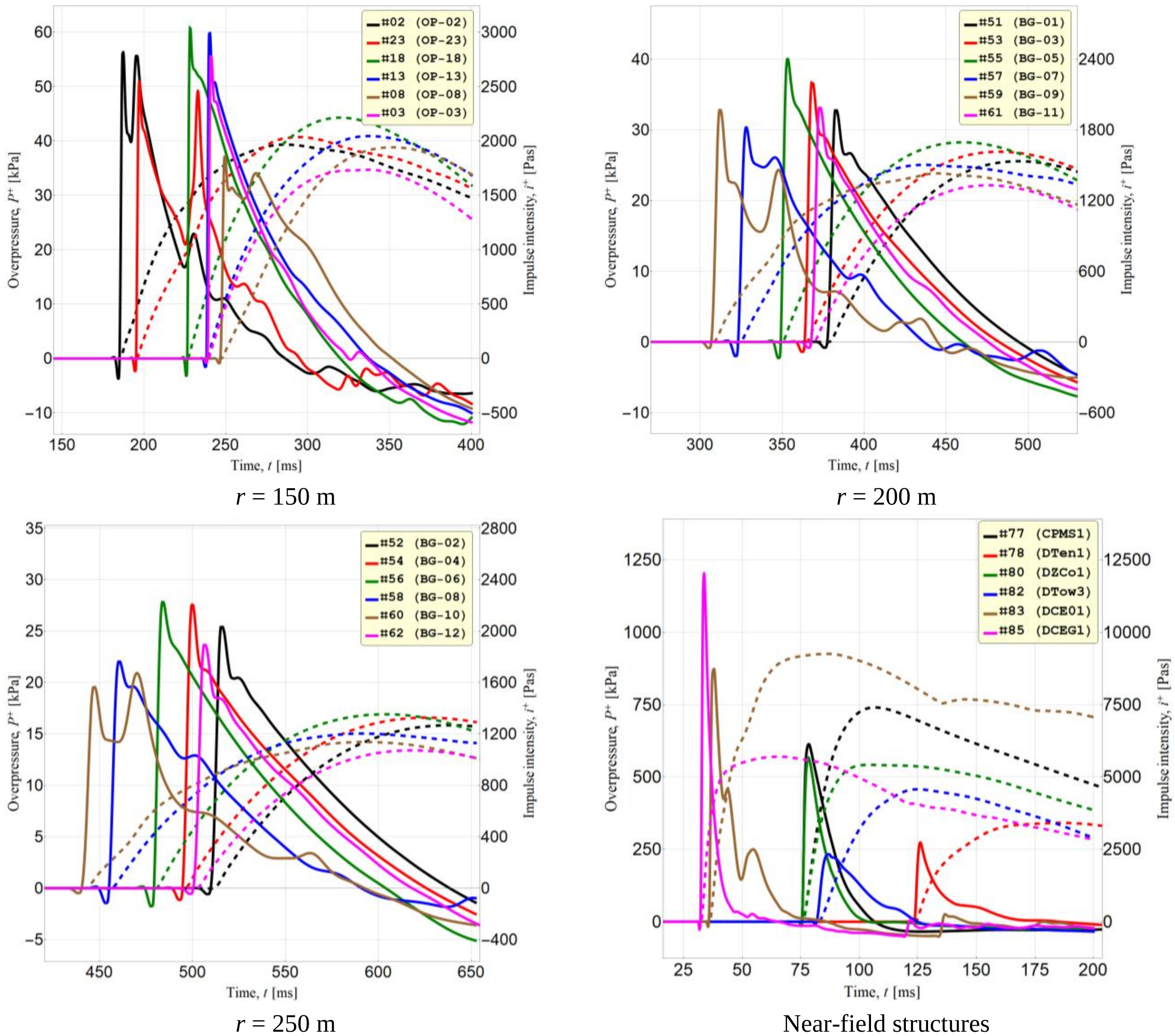


*Fig. 30 SHIELD test set-up; comparison of overpressure and impulse intensity for result points on ground at a distance 150-250 m from GZ and on near-field structures. See Fig. 25 to Fig. 28 for detailed location of result points.*

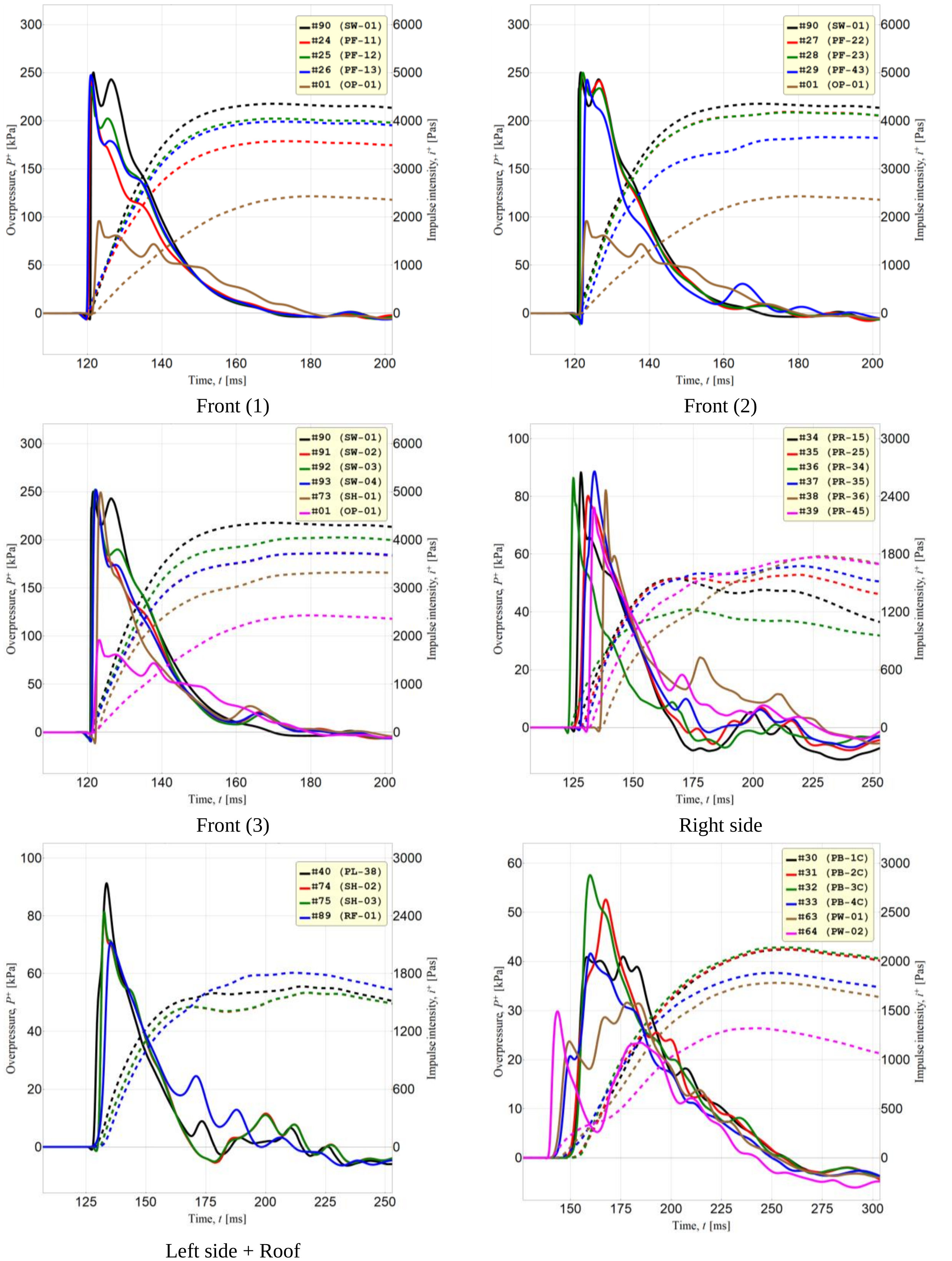


*Fig. 31 SHIELD test set-up; comparison of overpressure and impulse intensity for result points located at SKUSTA (front, sides and roof). See Fig. 11 for detailed location of result points.*

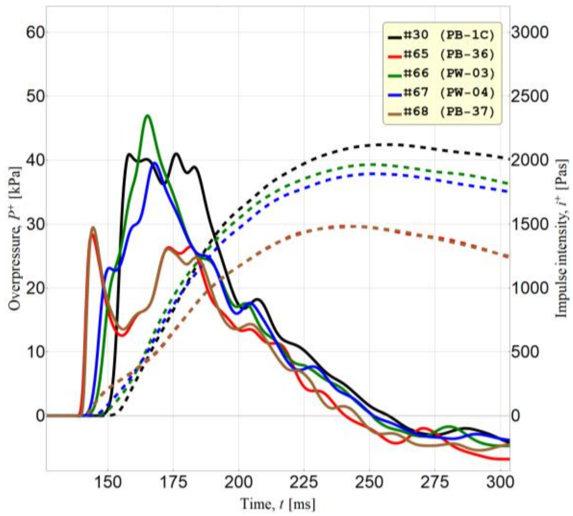


Back (1)

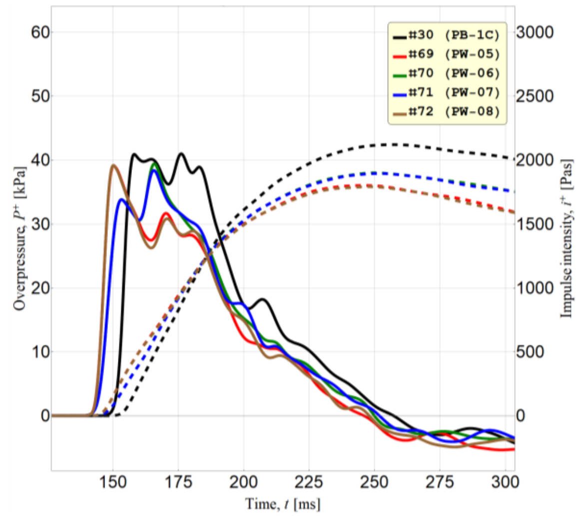


Back (2)

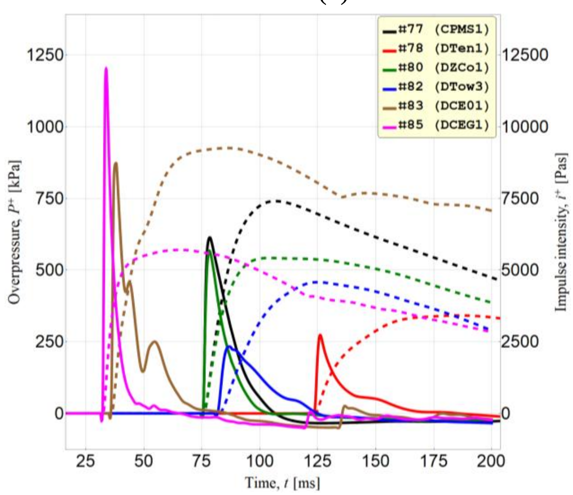


Back (3)

*Fig. 32 SHIELD test set-up; comparison of overpressure and impulse intensity for result points located at SKUSTA (back). See Fig. 11 for detailed location of result points.*